# IMPROVING THE UNDERWATER ACOUSTIC CHANNEL QUALITY VIA BEAMFORMING

by

Navid Eskandari

Submitted in partial fulfillment of the requirements
for the degree of Master of Electrical Engineering

at

Dalhousie University
Halifax, Nova Scotia
August 2018

*Dedicated to my parents, without whom non of my success would have been possible.*

# Contents

## List of Tables

## List of Figures

## Abstract

Underwater acoustic communication operates in one of the most complex wireless communication environments. Therefore, sophisticated signal processing techniques are required to make high-throughput communications possible. A typical acoustic channel has long impulse response and suffers from time variation caused by Doppler effects. In this thesis, we apply the delay-and-sum beamformer accompanied by multiple signal classification (MUSIC) algorithm to alleviate the harsh conditions of the underwater acoustic channel. Those proposed algorithms improve the channel power-delay profile and reduce Doppler spread causing channel taps variations.

Based on delay-and-sum beamformer and MUSIC algorithms, a poster and a conference paper were published.

• N. Eskandari, D, Trukhachev, C. Schlegel, "Underwater channel Beamforming technique" Wuwnet conference, Halifax, Canada, Nov.2017.
• N. Eskandari, M. Bashir, D. Truhachev, and C. Schlegel and JF. Bousquet "Improving the Quality of Underwater Acoustic Channel via Beamforming," *IEEE/MTS OCEANS*, Kobe, Japan, May 2018.

We have received constructive and encouraging feedbacks during and after the conference about our idea, which motivated us to continue and implement this technique on hardware in near future.

## Acknowledgements

Thanks to my parents who have helped me during my education, and my supervisors who gave me this opportunity to be part of this project and have helped me complete this project. Also, I want to thank all my friends.

# Chapter 1

# Introduction

The underwater acoustic communication channel is one of the most complex wireless communications channels due to rapid signal attenuation, high Doppler spread, long power delay profiles, limited bandwidth and limited transmission range. These are the most crucial factors introduced by the medium, which have to be dealt with for reliable communication under the surface of the seas.

The channel estimator whose task is to estimate and track the channel to extract the transmitted data from the received signal, faces significant Doppler spread which degrades estimator's performance. The estimator's performance is highly dependent upon the channel condition. If there was a way to alleviate channel taps with high Doppler, we could achieve better and more reliable underwater communication. Furthermore, the transmission data rate can be increased if there is a way to shorten long power-delay profiles.

Beamforming is a technique which has been used in many fields such as radar, biomedical engineering and wireless communications. This technique aims at maximizing the signal-to-interference ratio (SIR). Beamformer focuses on the angle of arrival of the desired signal, simultaneously, suppressing signals from other directions of arrival seen as interference.

In this thesis, we take a different point of view. Instead of maximizing signal-to-noise ratio (SNR), we shorten the channel impulse response. By means of beamforming, not only do we achieve better channel quality, but also data rate can be increased. Beamforming cures the communication channel defects and it has two significant results. First, our signal-to-interference ratio (SIR) increases, and second, beamformer application results in shorter channel power-delay profile by suppressing undesired arrivals with high Doppler.

## 1.1 Motivation

Based on the above noted channel issues, we were interested in applying a beamforming technique to solve them. The long channel power-delay profile, paths with high Doppler spread, and multi-path reduce the achievable data rate and cause difficulties in the underwater acoustics channel estimation and equalization, as mentioned in previous works on the underwater acoustics. Since our group works on designing an implementing a channel estimator for the underwater acoustic communications, there was a need to mitigate multi-path effect, and the paths with high Doppler causing the channel estimator deficiency. Therefore, beamforming was introduced as an individual project so that to tackle with those issues. Beamforming can lessen the effect of multi-path by suppressing the undesired paths, and we are not interested in receiving the paths which have high Doppler spread. In addition, the shorter the power-delay profile, the easier it is to equalize the channel. Because of medium characteristics, it is not possible to simply utilize large bandwidth to increase data rate. Thus, beamforming techniques are essentially needed for the underwater acoustics.

Also, we noticed that in the underwater acoustic experiments, we can decrease the transmitted signal power when beamforming techniques are used at the receiver, which is so important. Because most of the underwater devices are driven by batteries, and battery life is an important factor for long term experiments. In addition, lower SNR causes less harm to marine life.

## 1.2 Thesis Outline

In this chapter, we are going to look at some concepts which are common in wireless communications and needed for understanding of the next chapters. In the following chapter we take a look at transmission loss occurring in the underwater environment and study the link budget. In Chapter 3, the underwater channel and a simulated model for underwater communication experiments are discussed. Forth chapter is dedicated to a brief explanation of OFDM signaling. Chapter 5 explains different types of beamforming techniques and direction of arrival (DOA) estimation algorithms, and extensively discusses the delay-and-sum (DAS) beamformer and multiple signal classification (MUSIC) algorithm. The results based on real data and simulated versions of the underwater channel experiments are shown in this chapter, as well. In the

last chapter, the conclusion of this thesis and future work suggestions are given.

## 1.3 Multi-path Propagation

In wireless communications, the receivers receive multiple copies of the transmitted signal which arrive with delays. This effect is known as multi-path and present in the underwater communications. The reflection of acoustic signals from the surface and bottom, and the effect of spatially varying sound speed profile results in receiving many paths at the receivers [17]. Each path arrives with a delay and incident angle of arrival associated with it. An example of amplitude-delay profile of a simulated underwater channel is shown in Fig.1.1. These delays may lead to inter-symbol-interference (ISI). Multi-path and the resulting ISI limits the channel capacity.

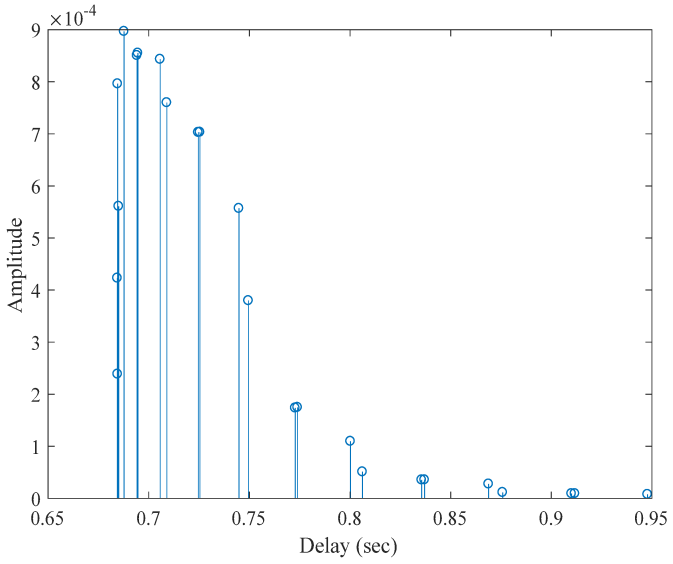


**Figure 1.1:** An example of amplitude-delay profile for an underwater channel.

## 1.4 Shadow Zones

Shadow zones are places under the surface of the seas, where the receiver can not receive any signal transmitted by the transmitter. Shadow zones may occur in short and long range communication, deep and shallow water acoustic communication, as well. Shadow zones are prompted by the sound speed profile of the channel resulting in sophisticated propagation of the acoustic signals. Fig. 1.2 shows the shadow zones.

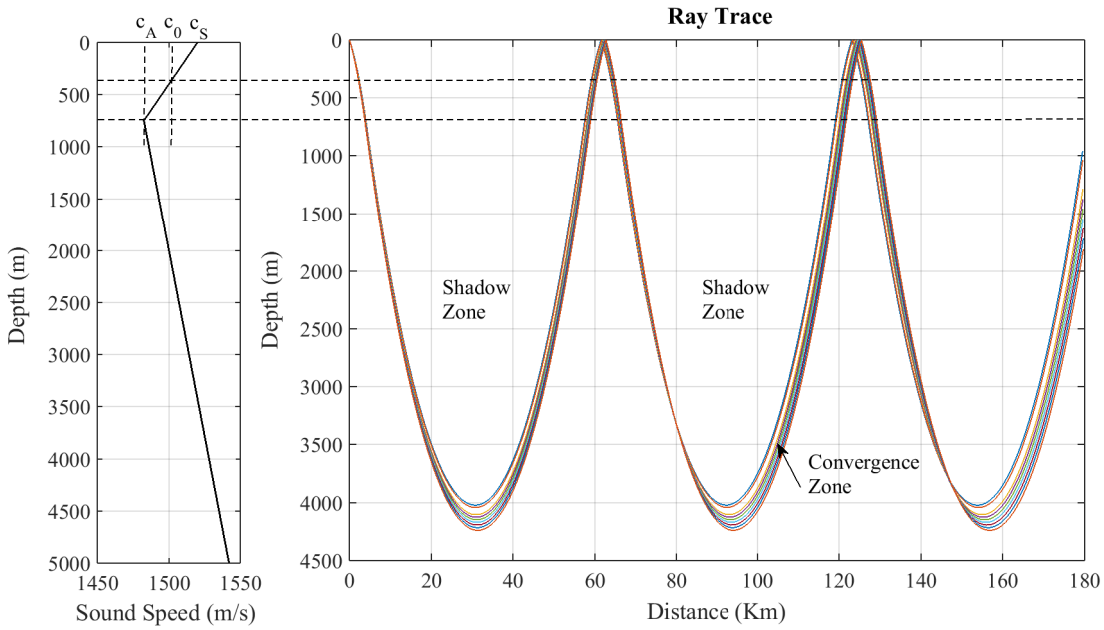


**Figure 1.2:** Shadow zone simulation based on a simulated sound speed profile [17].

## 1.5 Surface Scattering

Sea surface fluctuations are neither predictive nor the same for all paths. This effect causes a Doppler spread. The harsher the surface movements, the higher the Doppler spread is. Harsh surface also prompts more taps in channel power-delay profile due harsh surface scatters the paths in wider angles which then arrive at the receiver. In calm situations, the channel power delay shows some taps which are distributed sparsely [17].

## 1.6 Doppler Shift

Doppler shift is an effect caused by movement of either the transmitter or receiver, which prompts a shift in the spectrum of the signal and is common to all paths. There are effective ways to estimate and cancel this effect. Doppler shift is different for each path and depends on the incident angle.

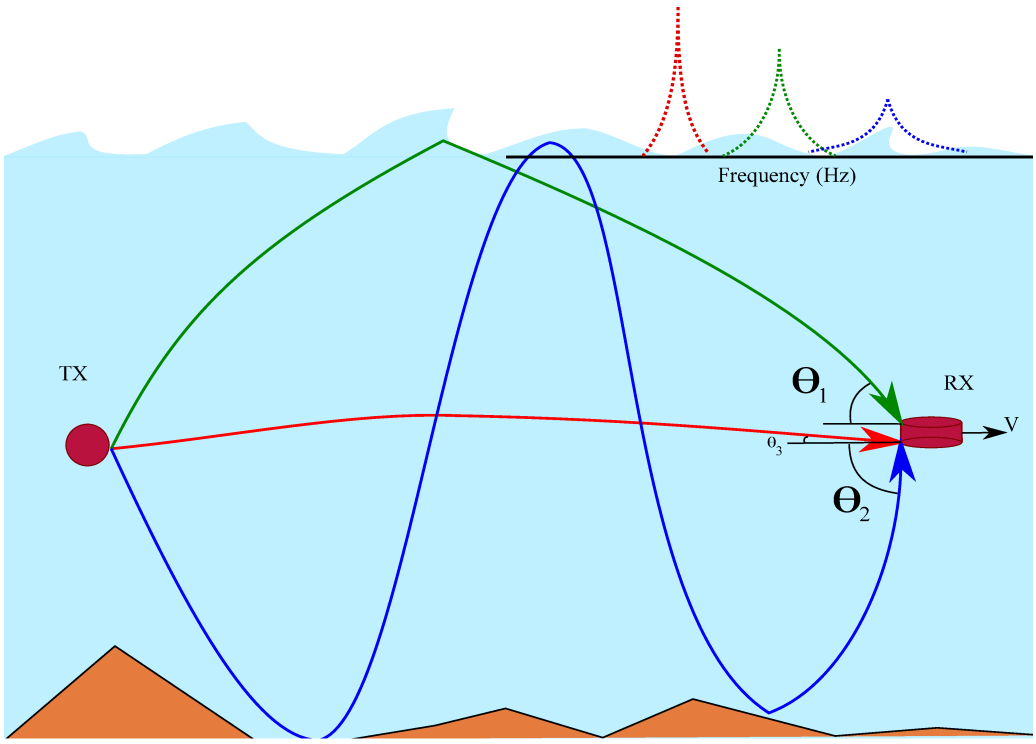


**Figure 1.3:** Different path at the receiver at time = $t_k$, and the Doppler spread associated with each path.

$$V_1 = V cos(\theta_1), \tag{1.1}$$

$$V_2 = V cos(\theta_2), \tag{1.2}$$

$$V_3 = V cos(\theta_3), \tag{1.3}$$

$$y(t) = \sum_{i=1}^{3} A_i cos(2\pi f_c(t + \frac{V_i t}{c}) + \tau_i), \tag{1.4}$$

$$y(t) = \sum_{i=1}^{3} A_i cos(2\pi f_c(1 + \frac{V_i}{c})t + \tau_i). \tag{1.5}$$

## 1.7 Doppler Spread

The fluctuation of surface and fading caused by waves result in another effect known as Doppler spread. This effect also is not the same for all paths due to number of bounces and surface fluctuation is different for each path. Therefore, we see a variation around the frequency taps in the frequency domain, as Fig. 1.3 shows. A model suggested that the paths with more signal bounces has wider Doppler spread [5].

The surface motion causes a distortion to the reflected acoustic signals. This distortion results in a multitude of micro Doppler-shifts effects which all together cause spread around the transmitted signal frequencies. As a result, it causes time-variation of both the signal power and fading.

## 1.8 Narrow-Band and Wide-Band Signaling

In communications, the relation between bandwidth and central frequency determines whether the system is narrow-band or wide-band. When the bandwidth is much smaller than the central frequency, that system is considered as narrow-band which is typically accepted in most terrestrial wireless communications. Wide-band systems, on the other hand, use more bandwidth for data transmission. The ratio between bandwidth and central frequency is considerable in these systems. The data rate in wide-band system is more than narrow-band systems. However, beamforming techniques are simpler for narrow-band systems than wide-band.

## 1.9 Literature Review

In the wireless communications, signals arrive at the receiver array with delays and angle of arrivals associated with each path. This phenomenon is known as multi-path. Some of the paths do not have good quality to estimate because of many reasons such as high Doppler spread. Therefore, there is a need to mitigate those low quality paths.

Some authors have suggested that beamforming techniques can alleviate the adverse multi-paths' effect and lessen the impact of undesired paths. In [2] and [3] different types of beamformers are discussed, which some highlights of them are reviewed in the following. There two types of beamformers discussed in documents and books. They are adaptive and non-adaptive beamformers. As table 4.1 in [2] shows there are different types of adaptive beamformers which have their own disadvantages.

Multiple side-lobe canceler (MSC) works in a way that it receives a signal from either one high gain main sensor or multiple sensors beamformed toward a specific angle, and the rest of the sensors act like auxiliary channels which are then multiplied by weight so that to cancel the

interference signals. it suppresses the interference signals. The disadvantage of this problem is the need for prior knowledge of where the desired signal is in order to steer beamformer's side-lobes toward undesired paths. The other algorithm is known as reference-signal (RS) which requires again the angle of arrival where the signal comes. However, if we know where the desired signal is, it will be easier to adapt a conventional narrow-band beamformer weights rather that using MSC or RS.

Delay-and-sum beamformer is very well known and robust beamformer. This beamformer itself is a non adaptive beamformer. However, by using direction of arrival (DOA) estimation techniques and adjusting weights with regard to DOA estimation results, it is possible to make it adaptive and steer toward desired angle of arrival.

Max SNR is an algorithm which steers its nulls and side-lobes toward the interference signals. This algorithm works with higher performance in comparison with MSC and reference signal. However, its performance may degrade when there are many interference signals in the received signal. Thus, we should look for better method which capable of handling multi-path channels.

In some wireless communication, the receiver receives multiple replicas of the transmitted signal, which are coherent with each other. This effect is known as multi-path. Some of the received paths have good quality. Therefore the beamformer should focus on them. Beamformers deal with steering vectors to steer toward the desired angle of arrival. Therefore, in some cases direction of arrival (DOA) estimation methods are used to find the angle of arrivals.

There are wide varieties of DOA estimation algorithms. Multiple signal classification (MUSIC) [13] [14], is one of them which has been used in many applications. It has been proven in many documents that this method is more efficient than the other method denoted as (ESPRIT) [21]. Some papers also have suggested the modified versions of MUSIC like root-MUSIC which enhances the MUSIC algorithm performance, but they still consider more number of sensors in the receiver array than number of received signals.

Coherence DOA estimation is also have been considered in some documents, such as spatial

smoothing [23] [24]. This method aims at processing coherent signal and achieve decoherent signal to find DOA. This method also reduces the channel rank. The main disadvantage of this method is the loss of array aperture. Hence, it requires more elements in the array. Although spatial smoothing increases DOA estimation precision, they use more number of receivers than number of received signals. Therefore, there still is a problem which has not been fully resolved.

Compressed sensing (CS) algorithm [25] is another method dealing with sparsity in the arrival signals. The CS algorithm aims at reconstructing the signal with fewer number of samples other algorithms use. It is proven that there are limited number of replicas of the transmitted signal in the received signal with different angles. In other direction of arrivals, the receiver captures noise. This kind of behavior is know as sparsity. In [26] author suggested Basis Pursuit algorithm for compress sensing. The author showed that this algorithm has better performance for signals with sparsity characteristics.

There is another algorithm which is proposed in [27]. They used compress sensing and independent component analysis (ICA) for multi-path channels, and showed that it has better performance than other algorithm. They can overcome one of the issues which The MUSIC algorithm has. MUSIC is prone to arriving angles which the signals arriving angles are too close to each other, MUSIC often can not estimate them properly. However, they showed that DOA estimator works perfectly when arriving paths are close to each other based on their simulations. Although, they showed improvement in DOA estimation, they considered more elements in the receiver array than number of arriving signals in their simulation.

Most of these papers simulated and concluded their results based on a condition which they consider fewer number of received signals in multi-path than number of sensors in the receiver array. In the underwater communication, based on ray tracing models Bellhop [8], it is possible to receive many taps of arrival. Therefore, we looked for a way to adapt conventional MUSIC with multi-path effect and limited number of hydrophones, in our case we consider only five hydrophones and 24 angles of arrival. The aim of this thesis is to find the high quality paths among all path. We look for the path which has the smallest Doppler spread and highest power. More details about this project are discussed in the following chapters.

# Chapter 2

# Link Budget

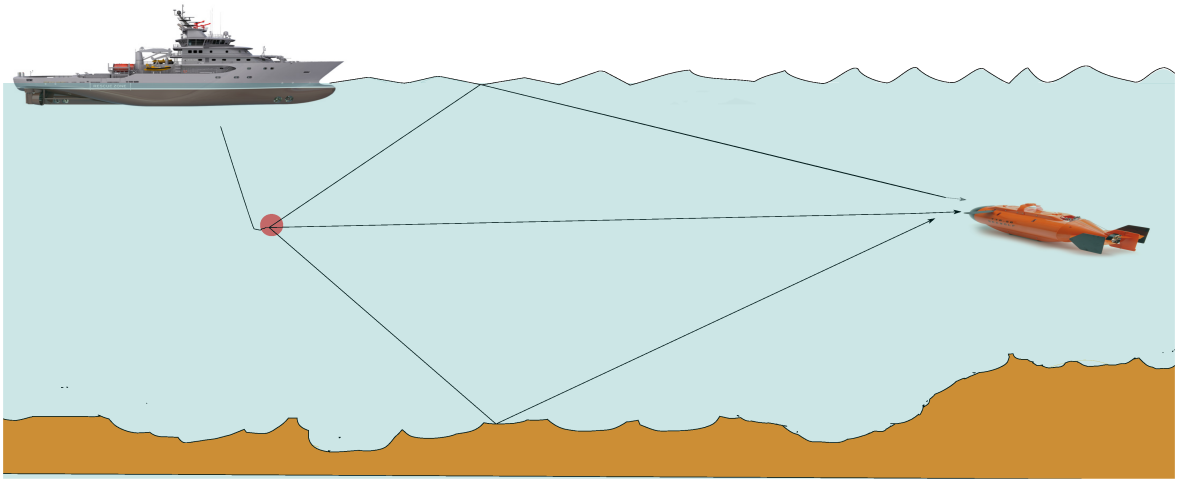

## 2.1 Introduction

The link budget is an important component in a communication system design. In underwater acoustic channels, we see different transmission effects such as delays and rapid signal attenuation stemming from a wide variety of factors. However, the main issue is the loss of power due to natural spreading of energy away from the source.

The received voltage at the receiver, $V_{Rx}$, depends on the transmitter voltage, $V_{Tx}$, and on $M_T$, $M_H$ which are the transducer and hydrophone conversion factors, respectively, and transmission loss represented by $L_{TL}$. These are related in the logarithmic domain as

$$V_{Rx} = V_{Tx} + M_T + M_H - L_{TL}. \tag{2.1}$$

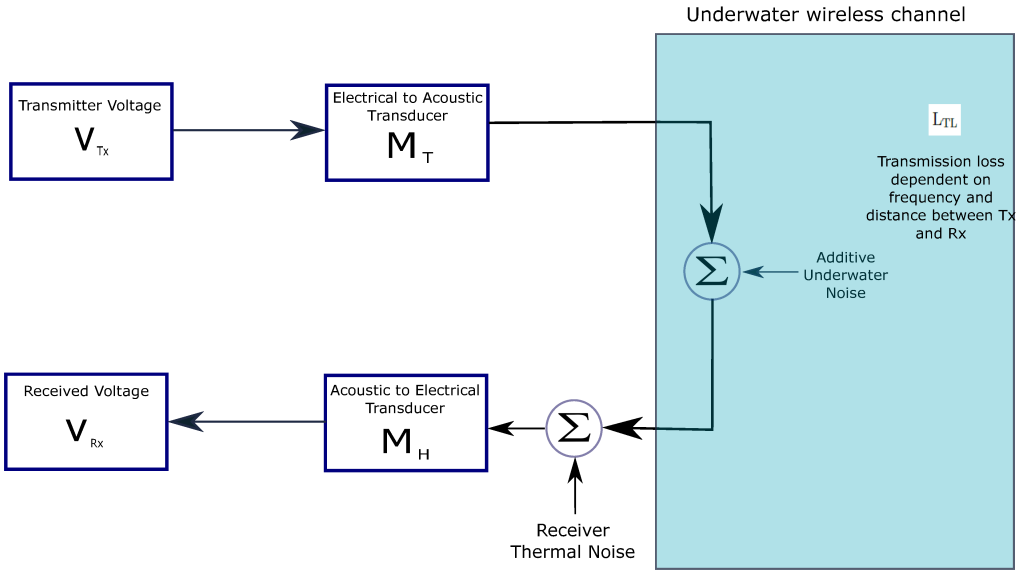


**Figure 2.1:** Illustration of an acoustic transmission

## 2.2 Sound Level

In order to transmit acoustic signals, we need transducers to convert an electrical signal into an acoustic signal. Transducers are mostly made of piezoelectric materials such as particular type of ceramics. By means of applying a voltage across a piezoelectric material, its shape is deformed. This deformation produces a volume change causing a pressure change in the surrounding medium that propagates as an acoustic wave. The typical value for this conversion factor denoted by $M_T$ is more than 120 dB relative to 1$\mu$Pa/V, where Pa denotes Pascal, (the amount of force in $N$ (newton) per unit area $m^2$) at the resonant frequency of the transducer which is around 28 kHz which is popular for commercial products.

At the receiver, a device known as hydrophone converts the local acoustic pressure called the sound pressure level (SPL), into an output i.e. a voltage. The acoustic signal intensity is measured in dB re 1$\mu$Pa, and SPL is calculated as

$$\text{SPL} = 20 \log_{10} V - M_H. \tag{2.2}$$

Since the piezoelectric devices can be modeled by an equivalent circuit consisting of capacitors, inductors and resistors, the SPL relates to the hydrophone output voltage V via $M_H$ which is the ratio between the open circuit output voltage and the pressure received by the hydrophone

[18]. The value for $M_H$ is on the order of 50 $\mu V$/Pa which in dB is $-206$ dB re $1V/\mu$Pa as shown in the picture below for four typical hydrophone sizes.

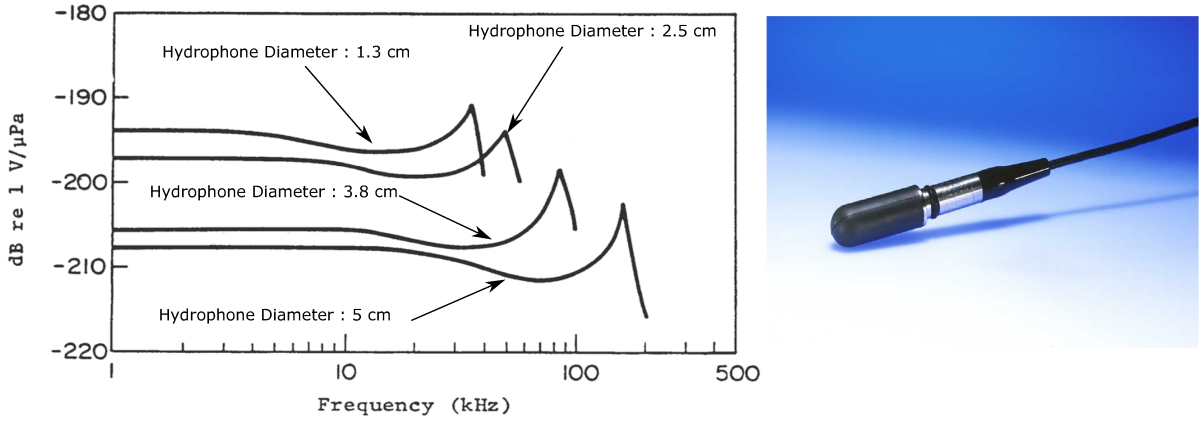


**Figure 2.2:** $M_H$ values for four typical hydrophones on the left, A typical hydrophone on the right

On the other hand, the source level (SL) at the receiver is the SPL 1 meter away from a source plus the transmission loss $L_{TL}$ related to the medium in which the acoustic signal travels. Eq. 2.2 in [18] describes it as,

$$\mathrm{SL} = \mathrm{SPL} + \mathrm{L}_{TL}. \tag{2.3}$$

### 2.2.1 Transmission Loss

The transmission loss is the ratio of the sound's intensity at the receiver, $I_1$, in comparison to intensity at 1 meter away from the source, $I_0$,

$$\mathrm{L_{TL}} = 10\log\left(\frac{I_0}{I_1}\right). \tag{2.4}$$

There are different sources of signal loss. The loss related to topology of the medium is called the spreading loss. There is also attenuation loss through the absorption of the energy.

#### Spreading Loss

**Spherical spreading** : When the water is deep enough such that it exceeds the distance between transmitter and receiver, we can consider spherical spreading of the acoustic energy. The spreading loss is then computed from the power flux identity as $4\pi \mathrm{r}_0^2 \mathrm{I}_0 = 4\pi r_1^2 \mathrm{I}_1$

$$\mathrm{L_{TL}} = 10\log\left(\frac{\mathrm{r}_1^2}{\mathrm{r}_0^2}\right) = 20\log\left(\frac{\mathrm{r}_1}{\mathrm{r}_0}\right). \tag{2.5}$$

**Cylindrical spreading:** If we are in shallow water or the distance between the source and receiver is longer than the water depth, we have the cylindrical spreading. Equality of power in different distances leads to $2\pi \mathrm{r}_0 \ell \mathrm{I}_0 = 2\pi \mathrm{r}_1 \ell \mathrm{I}_1$

$$\mathrm{L}_{\mathrm{TL}} = 10 \log \left( \frac{\mathrm{r}_1}{\mathrm{r}_0} \right). \tag{2.6}$$

### Absorption Loss

Absorption loss is caused by acoustic energy being converted into heat. It consists of three different effects, which mostly dependent on frequency:
(i) Shear viscosity causes signal loss, This is more apparent in sea than fresh water. Sea water shows this phenomena because of the chemical reaction of the dissolved salt in sea water.
(ii) Another factor that causes absorption is volume viscosity which arises from the time-lag that water molecules need to flow by means of the pressure into lattice holes in the crystal structure [6].
(iii) Ionic relaxation is the effect of magnesium sulfate ($MgSO_4$) that dissociates and re-associates under the pressure of acoustic signal. This is called *relaxation time*[6].
The following equations address all of the variables and was fitted to measurements. The former one is for spherical spreading and the later is related cylindrical spreading.

$$\mathrm{L}_{\mathrm{TL}} = 20 \log(r) + \alpha r \times 10^{-3} \tag{2.7}$$

$$\mathrm{L}_{\mathrm{TL}} = 10 \log(r) + \alpha r \times 10^{-3} \tag{2.8}$$

$$\alpha = \frac{0.11 f^2}{1 + f^2} + \frac{44 f^2}{4100 + f^2} + 3 \times 10^{-4} f^2. \tag{2.9}$$

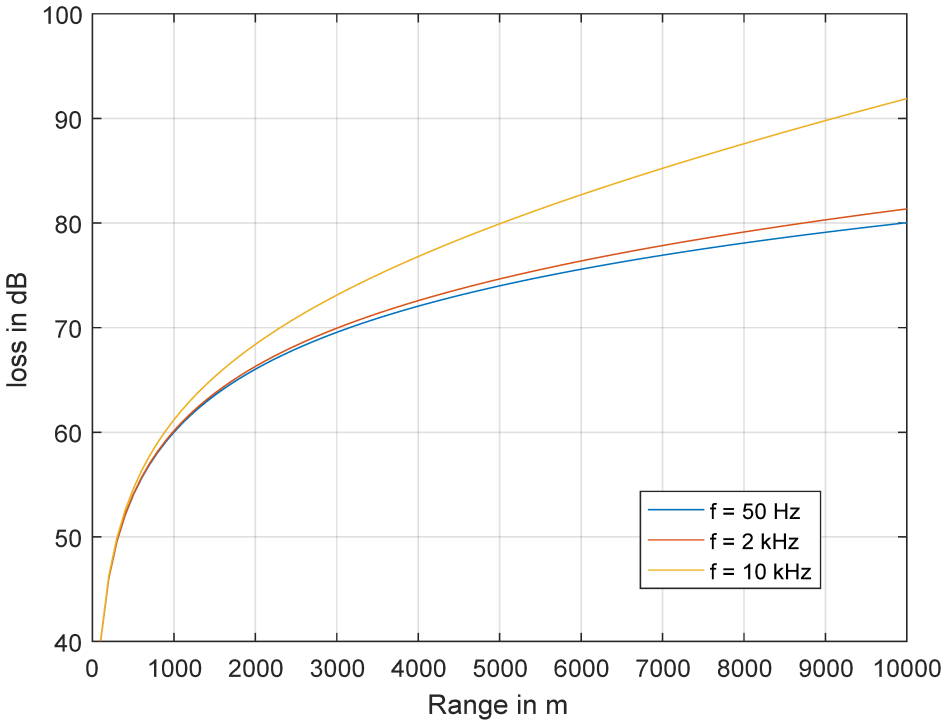


**Figure 2.3:** Transmission Loss related to spherical spreading and absorption loss

## 2.3 Underwater Noise

In order to obtain values for the signal-to-noise ratio (SNR) we need to factor in the different sources of underwater ambient noise, primarily turbulence, shipping, surface gravitational waves, and thermal receiver noise. The power spectral density of each noise source has been studied empirically in [19] , and are plotted in Fig. 2.4 with units of $\mu$Pa per Hz as a function of $f$ in kHz [19]. Each noise source dominates different portions of the spectrum. At frequencies below 10 Hz turbulence dominates; for frequencies between 10 and 100 Hz shipping activity becomes dominant and is modeled by the shipping parameter $s$ (where $0 < s < 1$). For frequencies ranging from 100 Hz to 100 kHz surface noise due to gravitational waves and determined by the wind speed $w_s$ is the dominant noise source, and at frequencies above 100 kHz thermal noise becomes the most important factor.

| Link Budget for 6 km Range and f=28 kHz | | |
|---|---|---|
| Transmitter Voltage | $V_{Tx}$ | 40 dB (100 $V_{RMS}$) |
| Transducer Conversion Factor | $M_{Tx}$ | 144 dB re 1 $\mu$Pa/V [20] |
| Transmission Loss | $L_{TL}$ | 145 dB |
| Noise PSD at f=28 kHz | $N_{PSD}$ | 20 dB re $\mu$Pa/Hz |
| Bandwidth | $B$=10 kHz | 40 dB |
| Signal Acoustic pressure/Noise Acoustic Pressure | $SNR$ | -20 dB |

**Table 2.1:** The link budget calculation example for 6 km range.

An example of link budget calculation is calculated and the value for each parameter is defined in the table for 9 km distance between transmitter and receiver.

$$SNR = V_{Tx} + M_T - L_{TL} - N_{PSD} - 10\log(BW) \tag{2.10}$$

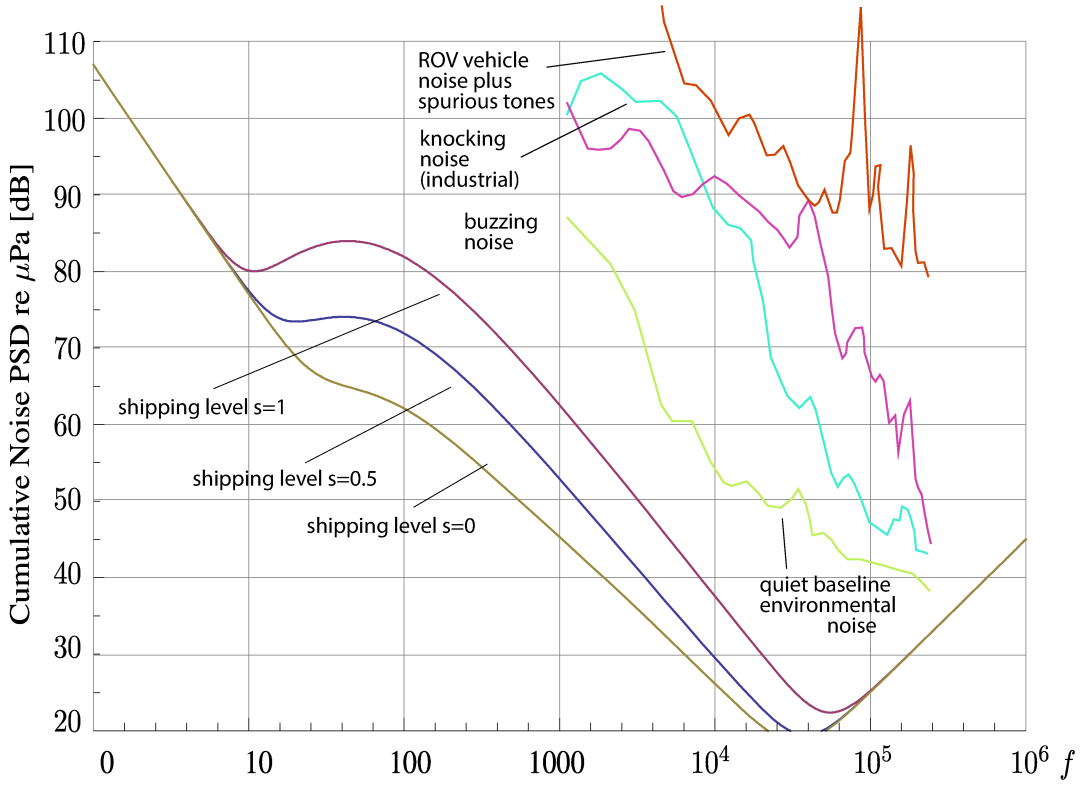


**Figure 2.4:** Example noise level in undersea acoustic channels [17].

# Chapter 3

# Underwater Channel Simulation

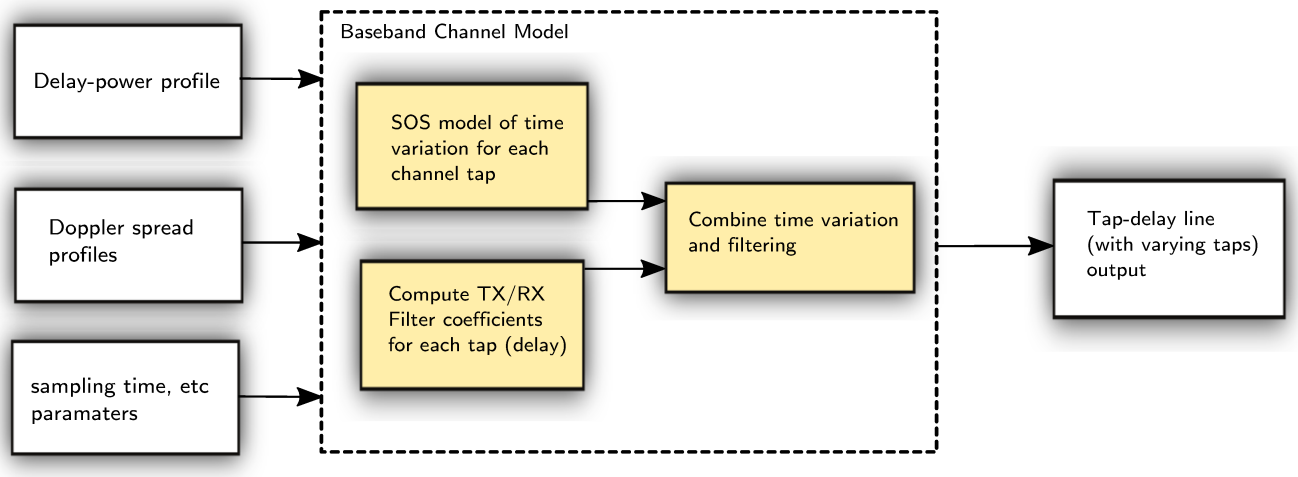


**Figure 3.1:** Channel modeling diagram.

In this chapter, we review the mathematics behind the underwater acoustic channel modeling, and model this channel based on parameters such as Doppler spread, power-delay profile, sampling time, and etc, as shown in Fig. 3.1. The model needs power-delay profile which can be generated either by an underwater channel simulator based on ray tracing software Bellhop [8] explained in this chapter or by the real experiment power-delay profile. In addition, the Doppler spread profile should be defined for the purpose of channel modeling. Bellhop [8] helps us find the simulated version of underwater channel power-delay profile, received and transmitted angles,

etc. These results are generated based on the information such as sound speed profile (SSP), frequency, depth of transmitter and receiver, number of transmitter and receiver elements and their separation distances, and the range between transmitter and receiver. We use the simulated channel data to produce underwater MIMO channel simulation by introducing sum-of-sinusoid (SOS) technique, and add Doppler to each path. Figures and data produced by Bellhop shown in this section are based on simulation done for real measurement in St,Margaret's Bay in Nova Scotia in 2017. Fig. 3.2 shows the area where the measurment was done.

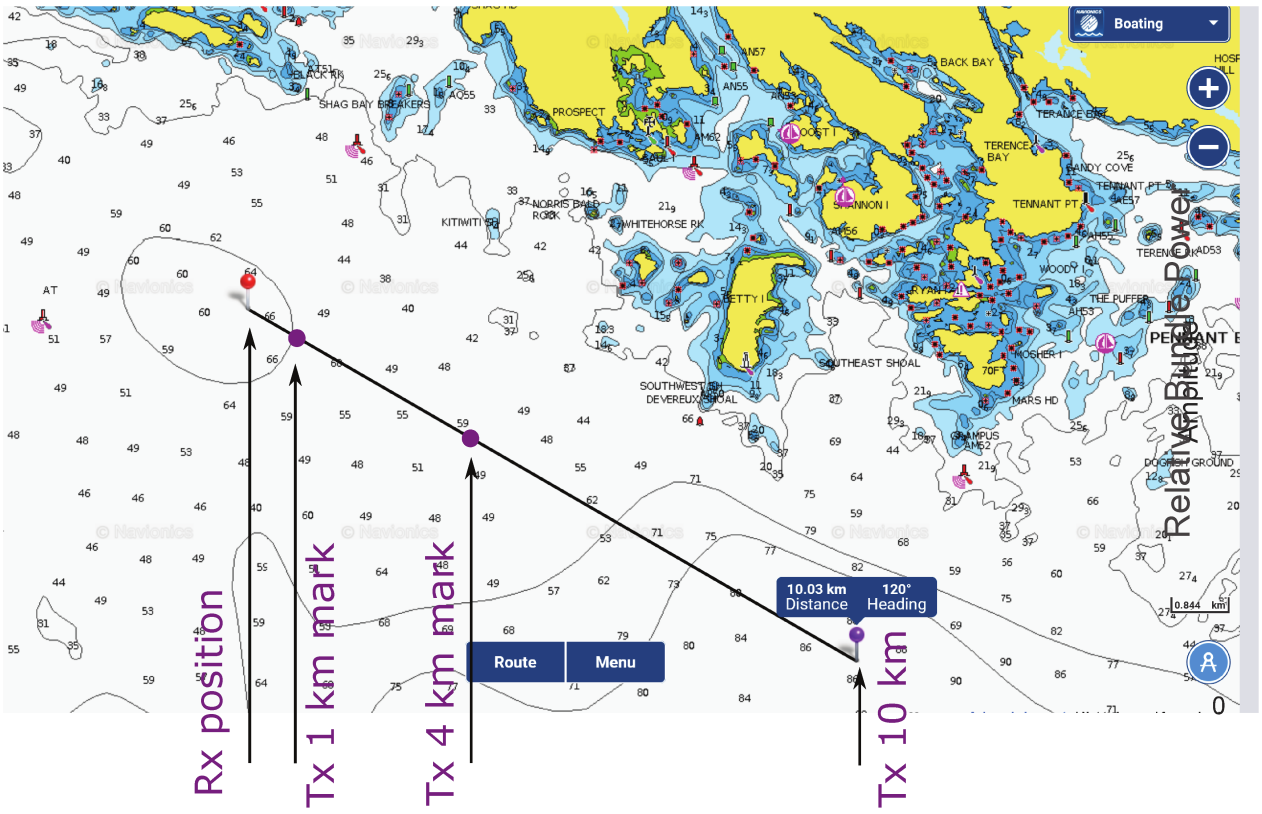


**Figure 3.2:** Map illustrates the area at where the real measurement was held in 2017.

## 3.1 Underwater Channel Characteristics

Wireless communication channels are mostly time dependent. The underwater acoustic channel can be considered as a linear time-varying channel. The channel impulse response in frequency

domain as a function of time is given as

$$H(f,t) = \sum_{p=1}^{P} h_p(t) e^{-j2\pi f \tau_p(t)}, \tag{3.1}$$

where, $h_p(t)$ and $\tau_p(t)$ are the amplitude and delay of path $p$, respectively. $H_0(f)$ represents the low-pass effect of the channel [17]. In the time domain, the channel impulse response in Eq. 3.1 can be modeled as

$$h(t,\tau) = \sum_{p=1}^{P} h_p(t)\delta(t - \tau_p(t)). \tag{3.2}$$

## 3.2 Sum-of-sinusoids ($SOS$) Channel Model of A Single Channel Tap

It is possible simulate an impulse response of a single-tap wide sense stationary uncorrelated scattering (WSSUS) channel, which is a function of scattering, via sums of sinusoids. This produces the time samples

$$h[i]_{rayleigh} = \frac{1}{\sqrt{M}} \sum_{m=1}^{M} e^{j(\phi_m + 2\pi f_m i T_s)}. \tag{3.3}$$

Where, $M$ is the number of sinusoids in the model, $\phi_m$ is an initial phase which is randomly and uniformly distributed in [0,2$\pi$]. $f_m$ is the frequency of sinusoids $m$ and accounting to Doppler spectrum. Alternatively,

$$h[i]_{Ricean} = \frac{1}{\sqrt{M(1+k_R)}} \Big( \sum_{m=1}^{M} e^{j(\phi_m + 2\pi f_m i T_s)} + \sqrt{K_R} e^{j(\phi_0 + 2\pi f_0 i T_s)} \Big) \tag{3.4}$$

where $K_r$ is the Rice factor, and $f_0$ is the Doppler shift frequency component.

In order to generate Equations 3.3 and 3.4, a limited number of Doppler frequencies, $M$, should be chosen to model Doppler spectrum function,

$$f(\nu) = \frac{1}{2\alpha} e^{-\frac{|\nu|}{\alpha}}. \tag{3.5}$$

By means of using the inverse transform sampling lemma, which states that the distribution of the output cumulative distribution function (CDF) $F(X)$, where X is opted with regard to $f(\nu)$,

is uniformly distributed between [0,1] [17]. Hence, it is possible to generate samples following $f(\nu)$ by choosing $y$ uniformly [0,1] and finding $x$ as

$$\nu = F^{-1}(y) \tag{3.6}$$

Therefore,

$$F(f_m) = \int_{-\infty}^{f_m} \frac{1}{2\alpha} e^{-\frac{|\nu|}{\alpha}} = \frac{\text{sgn}(f_m)}{2}(1 - e^{-\frac{|f_m|}{\alpha}}) \tag{3.7}$$

$$f_m = -\alpha \log \text{mod}(2u, 1)\text{sgn}(1 - 2u), \tag{3.8}$$

where $f_m$ is the Doppler frequency of the Doppler spectrum. $\alpha$ is the Doppler spread and mean relaxation frequency [1].

### 3.3 Modeling Multi-Path Channel using SOS

The underwater channel is a time-variant channel which is modeled in Eq. 3.2, where, $P$ is the total number of paths in the multi-path channel, $\tau_p$ is the delay associated with each path. $h_p(t)$ is the path amplitud which is a time-varying parameter and undergoes fading. In radio communication, there is an assumption that all $h_p(t)$ have the same Doppler spectrum [17]. This assumption is not correct in the underwater acoustics due to surface motions. Doppler spread is broader for paths which have multiple surface bounce. Eq. 3.2 is an infinite-bandwidth model because $\delta$ function is present in that equation. In communications, filters are used in transmitters and receivers for pulse shaping and limiting the bandwidth. Fig. 3.3 shows a communication channel with transmit and receive filters. Complex transmit samples $x_i$ are shaped by the transmit filter whose impulse response is $g(t)$. The medium affects the transmitted signal and causes multi-path, Doppler spread, and fading. The receive filter, $g^*(-t)$, receives and filters all the paths data [17]. The whole transmit, receive filtering and channel effect can be shown as

$$f(t, \tau) = h(t, \tau) \star g(\tau) \star g^*(-\tau) = h(t, \tau) \star g_{total}(\tau). \tag{3.9}$$

The received signal $z(t)$ is sampled at rate $T_s$ and given by

$$z(kT_s) = \sum_{j=k}^{k+l-1} x_j f(kT_s, (k-j)T_s) + n_k, \tag{3.10}$$

$$= \sum_{l=1}^{L} x_{k-l} f(kT_s, lT_s) + n_k. \tag{3.11}$$

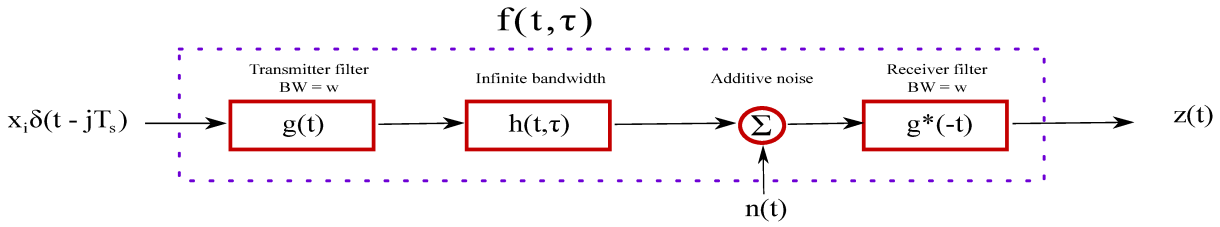


**Figure 3.3:** Multi-path fading channel, transmitter and received filters

Where, $k$ is discrete time index, $l$ is tap number, and $n_k$ is additive noise. Eq. 3.11 represents a tapped-delay line model of the resulting time-varying inter-symbol interference (ISI) [17].

## 3.4 Modeling Underwater Acoustics MIMO Systems

Modeling the underwater multi-input-multi-output (MIMO) is not trivial. Because the fading and multi-path behave differently in this medium. In this project, we focus on the beamforming aspect of the MIMO underwater acoustic communication.

In this model, we assume that the transmitter and receiver are stable. Therefore, the Doppler shift is not considered in the model. However, the Doppler spread stemming from surface fluctuations is considered. The Doppler spread parameter $\alpha$ depends upon the number of bounces a path has with the surface. The channel impulse response at hydrophone number $i$ is given by

$$h_i(t,\tau) = \sum_{p=1}^{P} f_{p,i}(t-\tau_{1,i})\delta(\tau-\tau_{1,i}-\tau_p), \tag{3.12}$$

$$\tau_{1,i} = \frac{d_{1,i}sin(\theta_p)}{c}, \tag{3.13}$$

where $\tau_{1,i}$ is the delay associated with hydrophone $i$ considering hydrophone number one as reference, $d_{1,i}$ is the distance between first hydrophone in the array and hydrophone number $i$, $\theta_p$ is the incident angle of arrival, and $c$ represents the sound speed [1].

This simulator is built upon the underwater acoustic channel power-delay profile which can be used either real sea trial channel power-delay profile or ray tracing model such as Bellhop [8]. In the following the ray tracing model, Bellhop, is discussed briefly.

## 3.5 Bellhop Ray Tracing Model

The Bellhop software [8], helps us find the channel power delay profile. Highlights of the software program are discussed in this section. For more details, refer to [8].

### 3.5.1 Sound-Speed Profile

The sound speed is not constant at different depth in water column. It varies with salinity, temperature, pressure, and depth [6]. Experiments also have shown that the sound speed changes in different seasons. All of these factors affect the an acoustic signal propagated under the water. The acoustic signal is bent as it is propagated throughout the medium. This phenomenon is known as refraction.

The sound speed profile should be defined in the environmental file in the Bellhop software for different depths. Fig. 3.4 illustrates a simulated sound speed profile for the location where real measurement was taken place in 2017. The point in Fig. 3.4 where the sound speed is approximately 1460 m/s, shows there is "duct" at 40 m depth. A duct forms at a depth where the sound speed around that point is symmetric. As Fig. 3.4 shows the sound speed is higher than 1460 m/s and there is similarity in the sound speed for both shallower and deeper depth around 40 m depth.

In some cases the duct forms at a depth that the signal is bent before hitting surface or bottom of the seas. Therefore, the acoustic signal propagated in that depth can travel to further distance without too much attenuation due to no bounce, due to each bounce reduces the acoustic signal energy. It means the sound can travel much longer distances [7].

### 3.5.2 Bathymetry

Bathymetry is another parameter that affects the power-delay profile significantly. The sea bottom profile can block rays and introduces shadow zones, where no transmitted sound is received. Moreover, the structure of the bathymetry itself has profound impact on the wave propagation, for instance, if the bottom is made of hard rock, reflections from the bottom will be stronger. On the other hand, if it is made of sand which absorbs sound energy quite considerably, the reflections will not be so strong and reduce more energy. Fig. 3.5 shows the bathymetry where

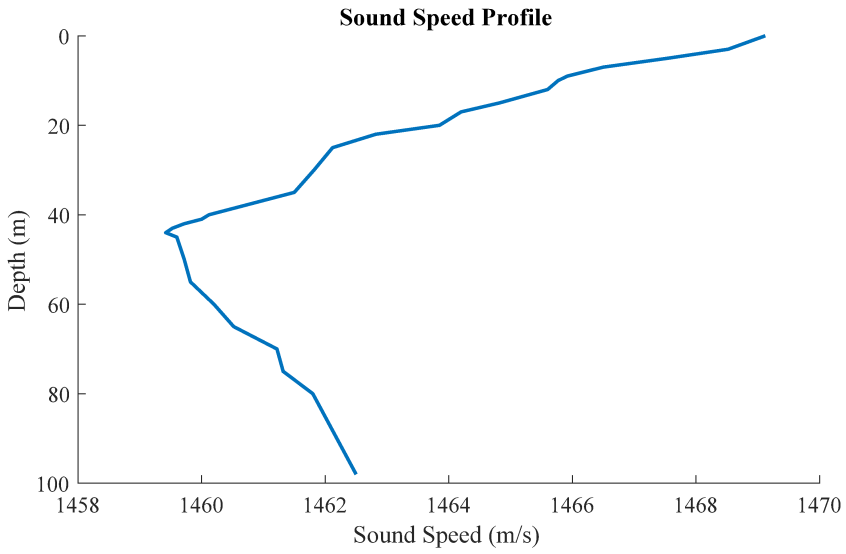


**Figure 3.4:** Sound speed profile

the measurement took place in July 2017 at St. Margarets Bay Nova Scotia.

Bellhop software has a parameter for sound speed at the bottom of the sea, which can be defined in .env file. The higher this number, the harder the bottom is defined.

### 3.5.3 Transmitter/ Receiver Configuration

The places where the transmitter and receivers are located are important parameters. It must be defined in Bellhop [8]. Sometimes it is possible the receiver does not receive any signal due to it is being located in a shadow zone. The transmitter, in this project, is assumed to be omni-directional, and beamforming is applied at the receiver where multiple hydrophones are used at the hydrophone array. The transmitter and receiver were placed around 40 meter depth in real experiment and the depth varied between 59 to 80 meter.

The spacing between hydrophones is an important parameter. It has been proven and mentioned in many documents that this distance should be less than wavelength, $\lambda$, in order to

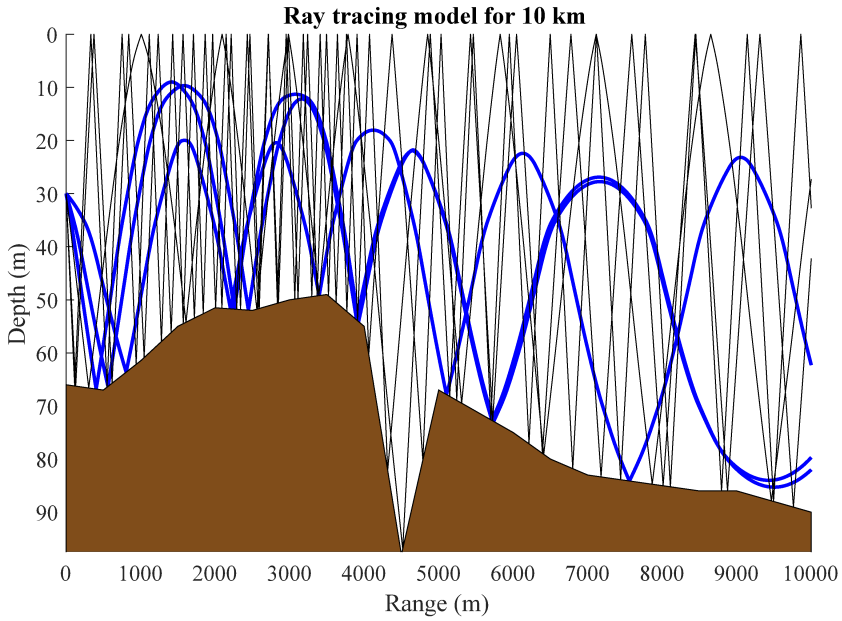


**Figure 3.5:** The sound propagation model based on the bathymetry of St, Margaret's Bay, simulated by Bellhop [8].

prevent grating lobe effect discussed in Chapter 5. The wavelength is defined as

$$\lambda = \frac{c}{f_C}, \tag{3.14}$$

where, $f_c$ is the central frequency of the passband signal, $c$ is the sound speed at the receiver. In all experiments, the spacing between hydrophones, denoted as $d$, is fix to 36 cm, because of 2048 Hz had been chosen as the central frequency. Although, in other experiments higher central frequencies have been chosen, the hydrophone spacing have remained constant in real experiments.

Range, the angles which the transmitter projects the sound and receiver receive the sound from those angles are parameters that must be defined before running ray tracing simulation.

### 3.5.4 Run Type Options

Bellhop can show simulation results in different representations based on the run type option defined in the environmental file. It can generate eigen ray figures showing the paths arriving

at a specific hydrophone, ray file demonstrates all the paths between transmitters and receivers based on the number of beams defined in the environmental file. The other types of run type options can be found in [8].

### 3.6 Matlab Results Based on Bellhop

Bellhop is a Matlab-based program. The most important information produced by Bellhop is the **arr_info** structure in Matlab. It contains the amplitudes, delays, transmit and receive angles and number of top and bottom bounces associated with each path.

The channel simulation aims at simulating the underwater MIMO channel system. It uses either the information which Bellhop produces or a channel power-delay profiles derived from real experiment, and produces a channel matrix $H$. Fig. 3.6 demonstrates the plots amplitude-delay profile and the amplitude-receiving angles profile based on Bellhop simulation.

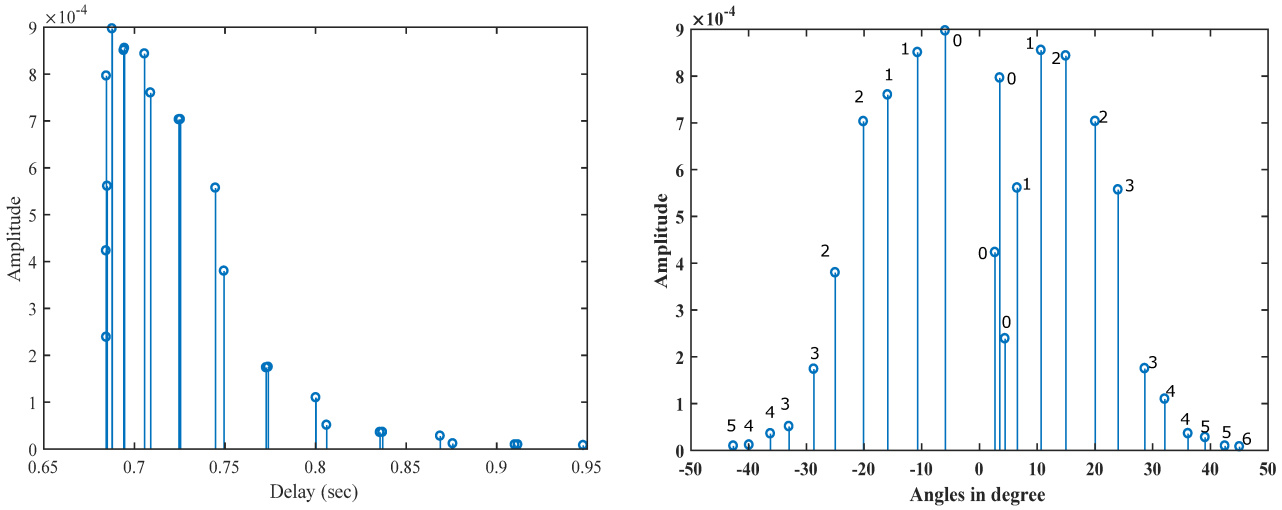


**Figure 3.6:** Amplitude-Delay profile on the left, amplitude-receiving angle profile, in which number of top bounces are written on top of each path, on the right.

## 3.7 Channel Simulation Result

A channel simulation based on Bellhop data is depicted in Fig. 3.7 and Fig. 3.8 showing the $H$ matrix with Doppler spread factors $\alpha = 0.1$ and $\alpha = 0.5$. The Doppler spread is a phenomenon which is bounce dependent [5]. Therefore the paths have more top bounces, have more variations.

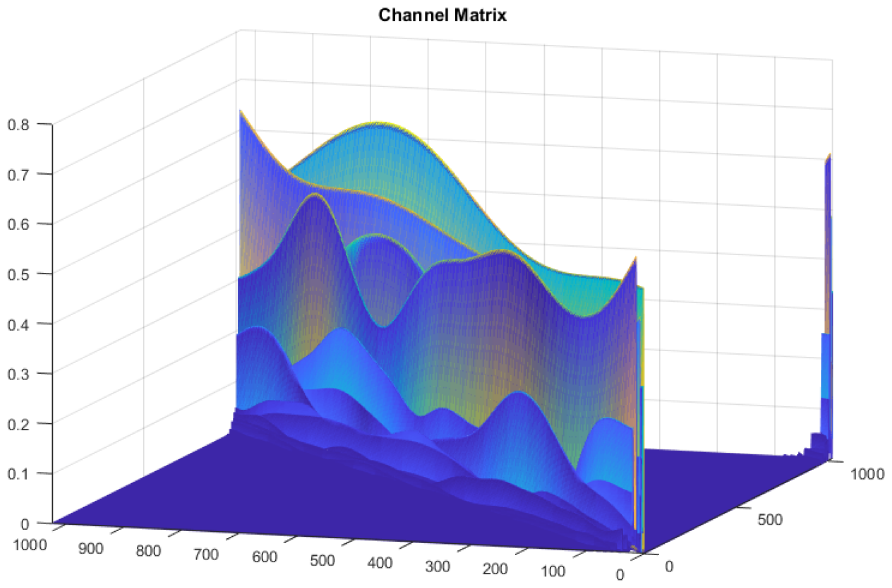


**Figure 3.7:** Absolute value of the channel matrix H. $\alpha = 0.1$

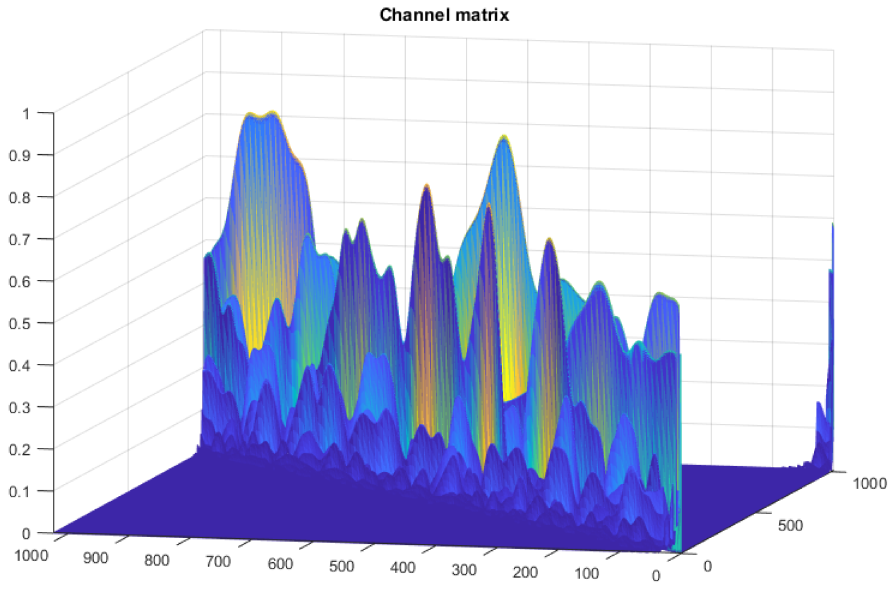


**Figure 3.8:** Absolute value of the channel matrix H. $\alpha = 0.5$

## 3.8 Channel Quality Parameters

There are two definitions which define the quality of communication channel. First, delay spread; the time difference between the first received path and the last one. Multi-path causes this effect. Average delay for both continuous and discrete are shown below.

$$\bar{\tau} = \frac{\int_0^\infty \tau\Phi(\tau)d\tau}{\int_0^\infty \Phi(\tau)d\tau}, \tag{3.15}$$

$$\bar{\tau} = \frac{\sum_k \tau\Phi(\tau)}{\sum_k \Phi(\tau)}, \tag{3.16}$$

where, $\Phi(\tau)$ is the amplitude associated with delay at time $\tau$. One of the most important usage of the average delay is RMS delay spread.

$$\psi = \sqrt{\frac{\int_0^\infty (\tau - \bar{\tau})^2\Phi(\tau)d\tau}{\int_0^\infty \Phi(\tau)d\tau}}, \tag{3.17}$$

$$\psi = \sqrt{\bar{\tau^2} - (\bar{\tau})^2}. \tag{3.18}$$

The RMS delay spread helps us define coherence bandwidth over which the frequency response of the channel is approximately constant. The coherence bandwidth is inversely proportional to the RMS delay spread.

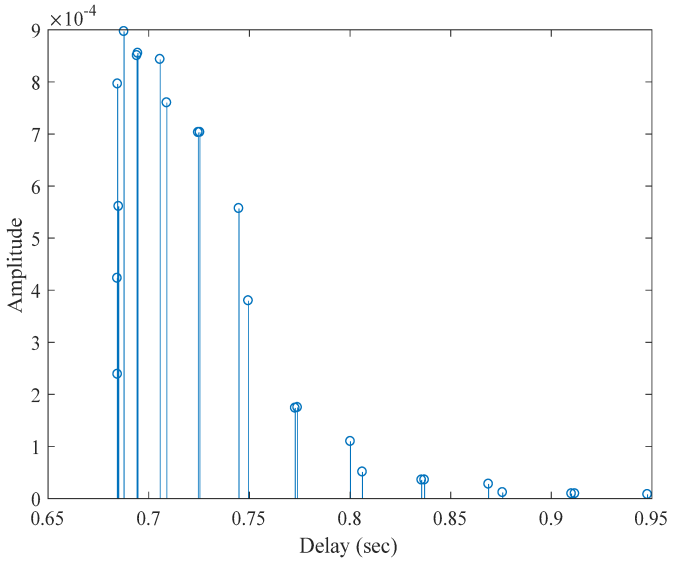


**Figure 3.9:** An example of a channel amplitude-profile for RMS delay calculation.

The other important parameter is the RMS Doppler spread. This factor quantifies the frequency spread around the central frequency. In underwater communications surface motion is a major cause for the Doppler spread. There is a very important factor in wireless communication known as coherence time. This factor inversely related to the Doppler spread. It defines the time duration which the channel is approximately constant.At the end of Chapter 5,RMS-delay and RMS-Doppler are computed for different real experiments.

# Chapter 4

# OFDM Signaling

Orthogonal Frequency Division Multiplexing (OFDM) signaling is one of the signaling methods that uses the bandwidth efficiently. OFDM divides the bandwidth into many smaller chunks which are called sub-carriers. This technique can help us send the data over multiple frequencies without degrading the signal quality. It has higher spectral efficiency than conventional frequency division multiplexing. Moreover, there is no need to utilize costly band-pass filters to separate the sub-carriers. OFDM, however, is vulnerable to fast fading and channel time variations. The other disadvantage is the high peak to average power ratio. However, in the recent years, amplifiers has advanced a lot to tackle this issue [17]. In our case, class D amplifiers are used. Low complexity of modulation and demodulation of the OFDM signaling outweigh its disadvantages. Additionally, the Fast Fourier Transform (FFT, iFFT) lessens the complexity of OFDM systems.

OFDM has been used in many types of wireless communication systems. Since wireless channels are often frequency-selective and deep fades occur in certain frequencies, OFDM helps us prevent losing the entire data frame in those frequencies if appropriate coding scheme is used for data transmission.

This signaling is based on the orthogonality of exponentials. In the baseband the bandwidth $W$ is divided into N (complex) sub-carriers. the frequency spacing between neighboring sub-carriers is defined as,

$$\Delta f = f_k - f_{k-1}, \tag{4.1}$$

where, $f_k = k\frac{W}{N}$, and $k = [0, N-1]$. There is another term known as symbol rate $r$ which can be defined as,

$$r = \frac{1}{T} = \Delta f = k\frac{W}{N}, \tag{4.2}$$

where, T is the symbol duration. Here, $W = 1/T_s$ where Ts is the equivalent single-carrier symbol time. Thus $T = NTs$, and $fk = k/T$ . The inner product of two modulated waveforms with different sub-carriers vanishes due to their orthogonality as mentioned in [17] and shown below,

$$\int_0^T e^{j2\pi f_1 t} e^{j2\pi f_2 t} dt = 0 \quad \text{if} \quad f_1 \neq f_2 \tag{4.3}$$

Equalization in OFDM signaling is simplified to a matrix multiplication in frequency domain. This is the most significant advantage of OFDM, which makes it suitable to be used as a standard signaling technique for radio systems, particularly for 4G LTE and 5G systems [17].

The analog base-band signal at the transmitter is given by

$$x(t) = \sum_{k=0}^{N-1} X[k] e^{j2\pi f_k t} = \sum_{k=0}^{N-1} X[k] e^{j2\pi \frac{k}{T_s} t} \tag{4.4}$$

where, $f_k = \dfrac{K}{T} = K\dfrac{W}{N}$ , $W$ is the total bandwidth in baseband. $X[k]$ carries the data in frequency domain and the received data in time domain can be sampled at rate $f_s = \dfrac{1}{T_s}$.

$$x(t) = x[nT_s] = x[n] \tag{4.5}$$

$$x[n] = \sum_{k=0}^{N-1} X[k] e^{j2\pi k \frac{W}{N} nT_s}; \quad n \in [0, N-1]. \tag{4.6}$$

It is apparent that the above equation is similar to the inverse Discrete Fourier Transform (iDFT). Thus, instead of dealing with an analog transceiver, a digital transceiver is preferred. Followed by the interpolation filter to convert the discrete time sequence to continuous time signal.

In order to utilize the bandwidth efficiently, $\dfrac{\sin(x)}{x}$ interpolation can be used as shown in Eq. 4.7. There, however, is better option to be used to alleviate the pre and post-cursor of the $\dfrac{\sin(x)}{x}$ function. A root-raised cosine filter, $g(t)$, with small roll-off factor $\alpha$ is preferred to eliminate excessive side-lobes in the time domain.

$$x(t) = \sum_{n=0}^{N-1} x[n]\text{sinc}\Big(\frac{t - nT_s}{T_s}\Big) \tag{4.7}$$

$$x(t) = \sum_{n=0}^{N-1} x[n]g(t - nT_s) = \sum_{n=0}^{N-1} x[n]g\Big(t - n\frac{T}{N}\Big) \tag{4.8}$$

We showed the signal in baseband; however, for long range transmission there is a need to up-convert the signal. The passband OFDM signal is given by

$$S(t) = Re\{x(t)e^{j2\pi f_c t}\} = x_i(t)\cos(2\pi f_c t) + x_q(t)\sin(2\pi f_c t), \tag{4.9}$$

where $x_i(t)$ and $x_q(t)$ are in-phase and quadrature component of the baseband signal, and $f_c$ is the carrier frequency.

Consider a vector of receive samples at the receiver represented by

$$\mathbf{y} = [y(T_s), y(2T_s), ..., y(NT_s)], \tag{4.10}$$

where, $T_s$ is the sampling period at the receiver. $\mathbf{y}$ carries the transmit signal containing both data and cyclic prefix,

$$\mathbf{x} = [cp, ..., cp, x(T), x(2T), ..., x(NT)]. \tag{4.11}$$

We can write a vector channel representation for the case of static multi-path channel as,

$$\mathbf{y} = \mathbf{H}\mathbf{x} + \boldsymbol{\psi}, \tag{4.12}$$

where $\mathbf{H}$ is the channel matrix in the frequency domain, as an example,

$$\mathbf{H} = \begin{bmatrix} f_1 & & & & f_L & \cdots & f_2 \\ \vdots & f_1 & & & & \ddots & \vdots \\ \vdots & \vdots & \ddots & & & & f_L \\ f_L & \vdots & \ddots & f_1 & & & \\ & f_L & \ddots & \vdots & f_1 & & \\ & & \ddots & \vdots & \vdots & \ddots & \\ & & & f_L & f_{L-1} & \cdots & f_1 \end{bmatrix}. \tag{4.13}$$

$$\mathbf{y} = \mathbf{F}^H y \tag{4.14}$$

$$= \mathbf{F}^H \mathbf{H} \mathbf{F}(x + \psi) \tag{4.15}$$

$$= \mathbf{H}^{(f)} \mathbf{X} + \mathbf{\Psi}. \tag{4.16}$$

where,

$$H^{(f)} = \mathbf{F}^H \mathbf{H} \mathbf{F} = \begin{bmatrix} H_0 & & & \\ & H_1 & & \\ & & \ddots & \\ & & & H_{N-1} \end{bmatrix} \tag{4.17}$$

is the diagonal frequency gain matrix [17].

$$y[n] = \frac{1}{\sqrt{N}} \sum_{k=0}^{N-1} H[k] X[k] e^{j2\pi k \frac{n}{N}} + \psi[n]. \tag{4.18}$$

By taking the DFT of y[n], we obtain

$$Y[K] = \frac{1}{\sqrt{N}} \sum_{k=0}^{N-1} y[n] e^{-j2\pi k \frac{n}{N}} = H[k] X[k] + \Psi(k). \tag{4.19}$$

To equalize we need to apply filter whose response is reciprocal to the channel frequency response, $H_f(e^{jw}) = \dfrac{1}{H(e^{jw})}$. It is possible to equalize the channel as,

$$\frac{Y[k]}{H[K]} = X[K] + \frac{\Psi(k)}{H[K]}. \tag{4.20}$$

The received signal, $\hat{X}$[k], is not exactly the same as the signal sent $X$[k], due to presence of the scaled noise, $\dfrac{\Psi(k)}{H[K]}$. Although the signal is corrupted by noise, it is sometimes possible to de-map the received data to achieve the constellation diagram and then retrieve the bit stream.

In fast fading channels, the channel matrix isn't diagonal [17]. Therefore, the channel matrix $\boldsymbol{H}$

modeled as,

$$\mathbf{H} = \begin{bmatrix} f_1[0] & & & & f_L[0] & \cdots & f_2[0] \\ \vdots & f_1[1] & & & & \ddots & \vdots \\ \vdots & \vdots & \ddots & & & & f_L[n-1] \\ f_L[n] & \vdots & \ddots & f_1[n] & & & \\ & f_L[n+1] & \ddots & \vdots & f_1[n+1] & & \\ & & \ddots & \vdots & \vdots & \ddots & \\ & & & f_L[N-1] & f_{L-1}[N-1] & \cdots & f_1[N-1] \end{bmatrix}. \tag{4.21}$$

### 4.0.1 Cyclic Prefix (CP)

Since our expected delay profile is quite long, we might receive a portion of previous transmitted symbol while receiving the desired symbol. This problem is known as Inter-Symbol-Interference (ISI). In order to tackle this problem, it is suggested to separate the symbols and put a guard time between them which is quiet. Thus, it is possible to stretch the signal by adding a portion of the signal tail to the beginning. This is called cyclic prefix (CP). Since, our estimator knows where the start of symbol is, that added portion can be discarded. Fig.4.1 depicts this method.

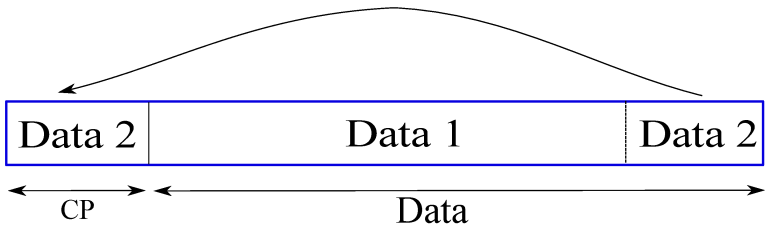


**Figure 4.1:** Cyclic prefix is a copy of OFDM data frame, which is attached to the beginning.

The cyclic prefix, however, reduces data rate due to the portion which the CP occupies could be used for the data. In addition, in underwater acoustics, the long delay profile requires longer CPs. Hence, shortening the channel helps use the smaller CP and use the bandwidth more efficiently.

### 4.0.2 Preamble and Pilots

Preamble is a set of known sequence which not only does help us extract the channel power delay profile by means of channel estimator, but can also be considered as synchronizer marker for the beginning of the symbol detection. It also can be used for beamforming purposes. Preamble consists of different pilots. For instance, in our experiments pilots are used to form a 64 size preamble. Pilots also do the same job with small difference. They are embedded inside the data or payload [17] . The transmit signal consists of the pilot comb shown below.

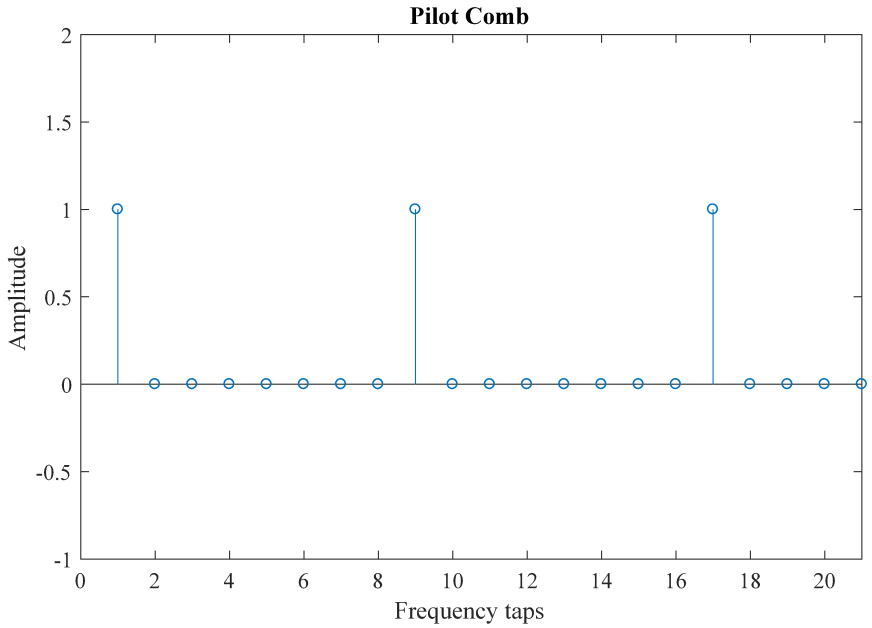


**Figure 4.2:** Pilot distribution in frequency domain

$$u(t) = \sum_{m} \alpha_m e^{j2\pi(f_c+\Delta f_m)t}. \tag{4.22}$$

Where, $u(t)$ transmitted signal, $m$ the number of OFDM signals, $\Delta f_m$ sub-carrier with regard to mth signal, $\alpha_m$ signal amplitude.

# Chapter 5

# Beamforming and Direction of Arrival Estimation Methods

As discussed in previous chapters, the underwater channel has long power-delay profile and paths with high Doppler spread. Improving the quality of underwater acoustic channel by removing the paths which have high Doppler spread, and curing the long channel power-delay profile are important goals on which this thesis is targeting. Beamforming techniques help us cure and improve the channel impulse response simultaneously. Some techniques require direction of arrival estimation. In this chapter, a section dedicated to some beamforming techniques with an emphasize on delay-and-sum (DAS) beamformer. Also, two methods for direction of estimation are discussed.

## 5.1 Beamforming

Beamforming techniques aim at maximizing the signal-to-interference (SIR) ratio. The beamformer focuses on a direction that the desired signal comes. There are many different types of beamforming methods which can be classified in different categories, but the adaptive and fixed (non-adaptive) beamforming techniques classification is widely used in both industry and academic papers. Both have their advantages and disadvantages which are discussed in this chapter. Before delving into beamforming techniques, it is appropriate to become familiar with array theory and some of the terminology used in this chapter.

## 5.2 Array Theory

A vertical hydrophone array receives a signal as a plane wave if the transmitter is located far enough from the receiver. The hydrophones in the array receive this wave with small delays associated with the distance between hydrophone $d$, and incident angle $\theta$ of the wave, as shown in Fig. 5.1.

Typically the distance $d$ is selected with regard to $\lambda$. Hydrophone spacing, $d$, should be less than wavelength, $\lambda$, due to presence of grating lobes in the receive array beam pattern if $d > \lambda$. Grating lobes are the lobes which have the same gain as the main lobe, but they are not steered toward the desired angle. Therefore, not only does beamformer not suppress those angles, but also it lets the undesired arrivals to be added to the desired signal without any attenuation, which is at odds with the main purpose of beamformer.

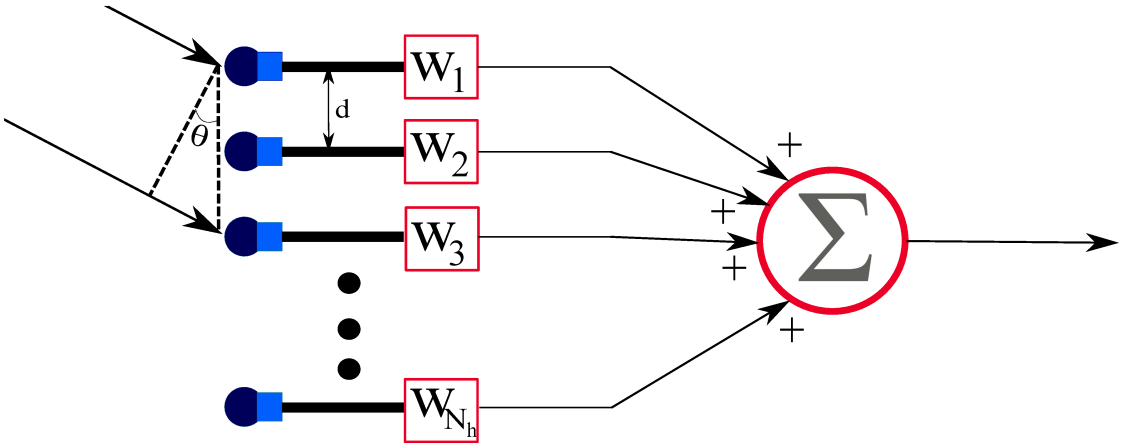


**Figure 5.1:** Hydrophone array

Beamformers are spatial to filters, and operate in the spatial domain rather than in time or frequency. Similar to filters, beamformers have a main-lobe with normalized unity gain, or 0 dB power at the peak, and it should normally be steered toward the angle of arrival of our desired signal. There is a -3 dB beam-width, analogous to bandwidth, where the beamformer attenuates more than 50 percent of the signal power. Its side-lobes power are less than 0 dB meaning that the signals going into the side-lobes are attenuated. Based on the number of elements, $N_h$, in the array, there is another term known as null which suppresses the signal considerably and eliminating the path which enters the null area owing to power attenuation are much larger than the side-lobes in places where nulls are occurred. There are $N_h - 1$ nulls in the beam pattern. A typical shape of beamformer is depicted in Fig. 5.3 and 5.2. It shows the shape for different frequencies.

The beam-pattern does not have identical shape for entire bandwidth for wide-band signals. Therefore, bandwidth range is an important parameter, due to narrow-band beamforming techniques are not suitable for wide-band signals. Narrow-band signals are considered in this thesis due to the algorithm used for direction of arrival estimation is a narrow-band algorithm. The maximum bandwidth which the beam-pattern has identical shape for all frequencies available in that bandwidth should be considered. In this thesis 500 Hz bandwidth is considered with 8 kHz central frequency is considered as narrow-band signal.

Before explaining different types of beamformer, it is needed to define how beamformers' main-lobes are steered toward specific direction. In all types of beamformers, whether fixed or adaptive, they use weights, as shown in 5.1, after each hydrophone at the receiver. These weights change the beam-pattern's shape. The goal of beamforming algorithm is to find appropriate weights that steer the main lobe toward desired angle.

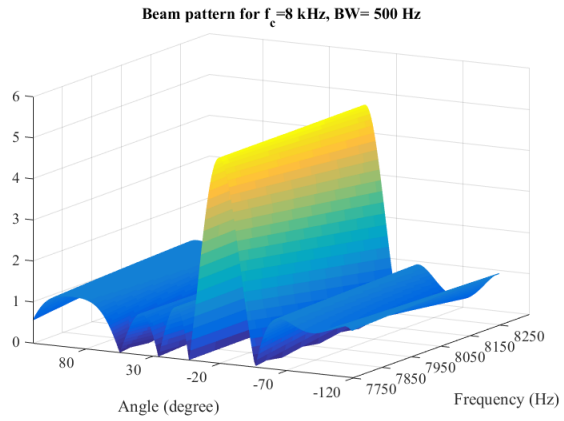


**Figure 5.2:** 3D view of typical shape of beamformer focusing at -20 degree, $N_h = 5$.

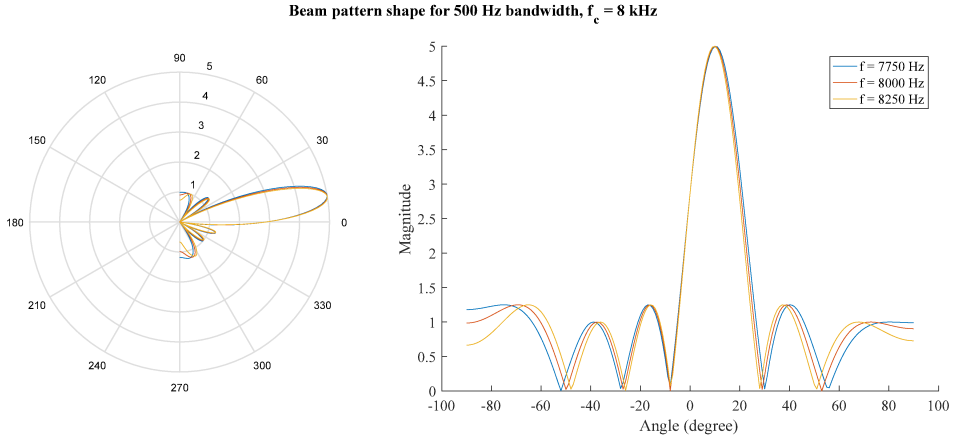


**Figure 5.3:** Typical shape of beamformer focusing at 10 degree, $N_h = 5$.

## 5.3 Fixed Beamformers

As the name indicates, these beamformers are fixed and focused on specific angle. They remain constant for an entire experiment without regard to communication channel variations during an experiment. This kind of beamformer is good for scenarios that the desired angles of arrival are known in advance. By means of multiplying appropriate constant weights to the receiver array elements, the main-lobe is focused on a specific angle and remains constant in that direction.

### 5.3.1 Delay-and-Sum Beamformer

Consider a single-input multiple-output (SIMO) underwater acoustic communication system where a baseband signal $x(t)$ is transmitted from a single transmit projector, and received by a vertical array consisting of $N_\mathrm{h}$ hydrophones. The hydrophones in the receiver array are equi-spaced, with distance $d$ meters between any two adjacent hydrophones. The carrier frequency is denoted by $f_c$ and the speed of sound in the water (assumed to be constant within the span of the array) is denoted by $c$.

If we consider a scenario that the channel has a single tap (is not frequency-selective) and the acoustic wave arrives at the receiver from an incident angle $\theta$ with delay $\tau$, the baseband

signals received by the $N_{\mathrm{h}}$ hydrophones are given by

$$y_i(t) = f^{(i)}(t)x(t - \Delta t_i - \tau) + n_i(t), \tag{5.1}$$

$$f^{(i)}(t) = f_{\mathrm{s}}^{(i)}(t)e^{j2\pi f_c \Delta t_i} \tag{5.2}$$

$$\Delta t_i = d\sin(\theta)(i-1)/c \tag{5.3}$$

where $i = 1, 2, \cdots, N_{\mathrm{h}}$ and the first hydrophone is used as the reference hydrophone when computing delays $\Delta t_i$. The time evolution (fading) of the channel tap itself at hydrophone $i$ is given by $f_{\mathrm{s}}^{(i)}(t)$, while $f^{(i)}(t)$ contains both time evolution and the frequency shift due to wave propagation from 1st hydrophone to $i$th hydrophone.

A narrow-band delay-and-sum (DAS) beamformer focusing onto incident angle $\theta'$ produces an output

$$y_{\mathrm{bf}}(t) = \boldsymbol{a}_{\theta'}^*(t)\boldsymbol{y}_{\mathrm{d}}(t) \quad \text{where} \tag{5.4}$$

$$\boldsymbol{y}_{\mathrm{d}}(t) = [y_1(t), y_2(t - \Delta t_2), \cdots, y_{N_{\mathrm{h}}}(t - \Delta t_{N_{\mathrm{h}}})]^{\mathrm{T}} \tag{5.5}$$

$$\boldsymbol{a}_{\theta'}(t) = [a_{\theta',1}(t), a_{\theta',2}(t), \cdots, a_{\theta',N_{\mathrm{h}}}(t)]^{\mathrm{T}} \tag{5.6}$$

$$a_{\theta',i}(t) = e^{j2\pi f_c d\sin(\theta')(i-1)/c} \quad i = 1, 2, \cdots, N_{\mathrm{h}} \tag{5.7}$$

where $\boldsymbol{a}_{\theta'}$ is a steering vector and $\boldsymbol{y}_{\mathrm{d}}(t)$ is a vector of delayed received signals. In case the beamforming angle $\theta' = \theta$ we obtain

$$y_{\mathrm{bf}}(t) = \boldsymbol{a}_{\theta}^*(t)\boldsymbol{y}_{\mathrm{d}}(t) = x(t - \tau)\sum_{i=1}^{N_{\mathrm{h}}} f^{(i)}(t + \Delta t_i)\ . \tag{5.8}$$

Consider now a multi-path channel with $L_{\mathrm{p}}$ signal propagation paths (see Chapter 3 for a detailed description of the channel model). Given the sampling time $T$ and the combined transmit-receive filter impulse response $g_{\mathrm{total}}(t)$ as well as the sequence of the discrete transmit signal samples $x_k = x(kT)$, $k = \cdots, 1, 2, 3, \cdots$ the received signal observed at the hydrophone $i$ is given by

$$y_i(t) = \sum_{p=1}^{L_{\mathrm{p}}} f_p^{(i)}(t)x(t - \Delta t_{i,p} - \tau_p) + n_i(t), \tag{5.9}$$

$$= \sum_{k=-\infty}^{\infty}\sum_{p=1}^{L_{\mathrm{p}}} f_p^{(i)}(t)g_{\mathrm{total}}(t - \Delta t_{i,p} - \tau_p - kT)x_k + n_i(t), \tag{5.10}$$

where, $i = 1, 2, \cdots, N_{\mathrm{h}}$, and the first hydrophone is used as the reference hydrophone when computing delays

$$\Delta t_{i,p} = d \sin(\theta_p)(i-1)/c \ . \tag{5.11}$$

The DAS beamformer (5.8) can then be applied to respective $y_{\mathrm{bf}}(t)$ sampled at the receive hydrophones.

## 5.4 Adaptive Beamformers

Since in wireless communication the channel is time-varying, non-adaptive beamformers may not be suitable for communications. Therefore, there is a need for a beamformer which adapts itself as the channel varies. Adaptive beamformers are classified into two categories: The first group is called blind beamformers, since they use no prior information about the spatial signature of the desired signal. Spatial signature isa response vector of a hydrophone array coming from a certain angle of arrival, for more information regarding this topic please refer to [22]. Thus, there is a need for training with known signals to form the beamforming weights. Some adaptive beamforming techniques require the spatial signature of the signal to steer toward the desired signal. Thus, there is a need for an algorithm which helps the beamformer find the angle of arrival. This process is known as direction of arrival estimation. In this section, algorithms for blind beamforming and direction of arrival methods are discussed.

### 5.4.1 Minimum Mean Square Error (MMSE) Beamformer

MMSE is a blind adaptive beamformer technique, and known as Wiener filter. The aim of this algorithm is to minimize the error $e(t)$ between the received and reference signals $P$. That reference signals in our case are a sequence of preambles, denoted as $P$ in this thesis. They are known and defined for the receiver in advance. The weights $\mathbf{w}$ are chosen as

$$\arg\min_{\mathbf{w}} \mathbb{E}\{|e(t)|^2\} = \arg\min_{\mathbf{w}} \mathbb{E}\{|\mathbf{w}^H S(t) - P|^2\} \tag{5.12}$$

$$\mathbb{E}\{|\mathbf{w}^H S(t) - P|^2\} = \mathbb{E}\{\mathbf{w}^H S(t) S^H(t)\mathbf{w} - \mathbf{w}^H S(t) P^* - S^H(t)\mathbf{w}P + PP^*\} \tag{5.13}$$

$$= \mathbf{w}^H \mathbf{R}\mathbf{w} - \mathbf{w}^H \mathbf{r}_{sp} - \mathbf{r}_{sp}^H \mathbf{w} + PP^* \tag{5.14}$$

where,

$$\mathbf{R} = \mathbb{E}\{S(t)S^H(t)\} \tag{5.15}$$

$$\mathbf{r}_{sp} = \mathbb{E}\{S(t)P^*\} \tag{5.16}$$

$$\frac{\partial\, \mathbb{E}\{|e(t)|^2\}}{\partial \mathbf{w}^H} = \mathbf{R}\mathbf{w} - \mathbf{r}_{sp} = 0 \tag{5.17}$$

$$\mathbf{w}_{MMSE} = \mathbf{R}^{-1}\mathbf{r}_{sp}. \tag{5.18}$$

Computing the weights for this technique requires significant time, which is a disadvantage. However, This technique does not depend on signal features, such as wide-band or narrow-band.

Other algorithms such as direction of arrival (DOA) estimation methods can alleviate the disadvantage of non-adaptive beamformers, and help them adapt their weights. DOA algorithm estimates the angle where the desired signal is received, and the beamformer adjusts its weights with regard to the estimated angle. In the following DOA methods are discussed.

## 5.5 Direction of Arrival Estimation

Some beamforming techniques, such as delay-and-sum beamformer, require knowledge of the spatial signature of the arriving signal prior to adapting the beamforming weights. Thus, estimating the angle of arrival is necessary. ESPRIT and MUSIC algorithms [13] [14] [21] are two DOA estimation methods which are going to be discussed in this chapter.

In order to apply beamforming techniques in underwater acoustics, a hydrophone array must be used. An underwater hydrophone array consists of multiple hydrophones at the receiver side. A signal arriving from an angle impinges on each hydrophone with delay and phase change associated with the hydrophone spacing distance $d$, as shown in Fig 5.4. Multi-path propagation causes to receive multiple copies of a signal from different angles. There is a Doppler spread and delay associated with each path. The paths with lower Doppler spread are easier to estimate.

We consider OFDM signaling with central frequency $f_c$, and each OFDM sub-carrier is considered as a narrow-band signal. In communication systems, when the bandwidth is much

smaller than central frequency $f_c$, it is called narrow-band system. In our case, 500 Hz bandwidth is considered narrow-band when the central frequency is 8 KHz or higher.

The aim of the direction of arrival (DOA) estimation is to find the spatial signature of the receiving signals and train the beamformer to steer toward the angle carrying signal with higher energy and lesser Doppler spread. There are different algorithms for DOA estimation covered in this chapter, with an emphasize on multiple signal classification (MUSIC). Results based on MUSIC are presented in this chapter, as well.

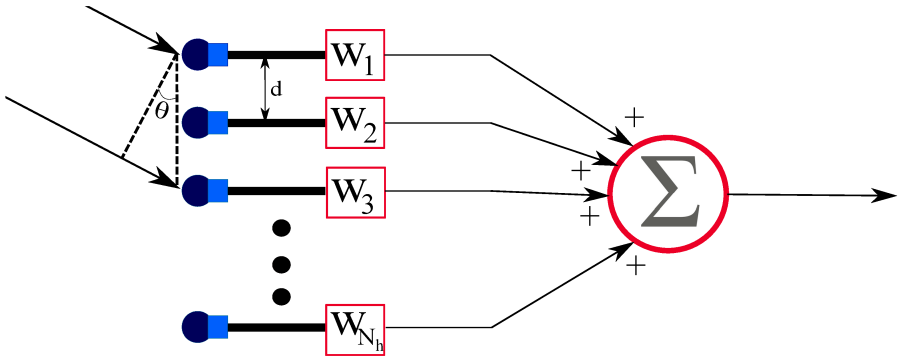


**Figure 5.4:** Hydrophone array

## 5.6 DOA Estimation Techniques

There are many direction of arrival algorithms that have been used in many fields of studies. Two of them are widely used and compared in publications. First, we explain the ESPRIT algorithm [21], and then, we delve into MUltiple SIgnal Classification (MUSIC) [13][14]. Both of these techniques deal with covariance matrix **R** of the signals received by different sensors, which in our case hydrophones act like sensors. The definition of covariance matrix is explained in Eq. 5.25.

### 5.6.1 Estimation of Signal Parameters using Rotational Invariance Techniques (Esprit)

ESPRIT is a DOA estimation algorithm that is based on the fact that if the received signal's steering vector formed as **A**,

$$\mathbf{A} = [\boldsymbol{a}_1^T(\theta), \boldsymbol{a}_2^T(\theta), ..., \boldsymbol{a}_i^T(\theta), ..., \boldsymbol{a}_M^T(\theta)], \tag{5.19}$$

$$\boldsymbol{a}_i(\theta) = [1, z^{-1}, ..., z^{-k}, ..., z^{-(N_h-1)}], \tag{5.20}$$

$$z^k = e^{j2\pi f_c k \frac{dsin(\theta)}{c}}. \tag{5.21}$$

Where, $f_c$ is the carrier frequency, $k$ is hydrophone number, $d$ is distance between two consecutive hydrophone, and $c$ is the sound speed. The steering matrix, $\mathbf{A}$, should be divided into two $(N_h - 1) \times M$ sub-matrices,

$$\mathbf{A}_0 = \begin{bmatrix} 1 & 1 & .... & 1 \\ z_{\theta_1}^{-1} & z_{\theta_2}^{-1} & ... & z_{\theta_M}^{-1} \\ z_{\theta_1}^{-2} & z_{\theta_2}^{-2} & ... & z_{\theta_M}^{-2} \\ . & . & ... & . \\ . & . & ... & . \\ . & . & ... & . \\ z_{\theta_1}^{-(N_h-2)} & z_{\theta_2}^{-(N_h-2)} & ... & z_{\theta_M}^{-(N_h-2)} \end{bmatrix}, \tag{5.22}$$

$$\mathbf{A}_1 = \begin{bmatrix} z_{\theta_1}^{-1} & z_{\theta_2}^{-1} & ... & z_{\theta_M}^{-1} \\ z_{\theta_1}^{-2} & z_{\theta_2}^{-2} & ... & z_{\theta_M}^{-2} \\ . & . & ... & . \\ . & . & ... & . \\ . & . & ... & . \\ z_{\theta_1}^{-(N_h-1)} & z_{\theta_2}^{-(N_h-1)} & ... & z_{\theta_M}^{-(N_h-1)} \end{bmatrix}. \tag{5.23}$$

These two matrices are related as, $\mathbf{A}_0 = \mathbf{A}_1\Phi$, where $\Phi$ is a diagonal matrix. Its diagonal values $\text{diag}(\Phi) = [u_1, u_2, ..., u_j, ..., u_M]$ show the phase shift associated with each individual arriving path received by the hydrophone array. Thus, if it is possible to estimate these diagonal values, the angles of arrival for each individual element and path can be found using,

$$\cos(\phi) = c\frac{\ln(u_j)}{kdf_c}. \tag{5.24}$$

We do not have access to $\mathbf{A}_0$ and $\mathbf{A}_1$ though. Thus, we use the received data $y$, introduced in the Chapter 3 to form covariance matrix $\mathbf{R}$ [21], shown in Eq. 5.25, and apply eigen value

decomposition $\mathbf{Q}_s$, mentioned in Eq 5.26 as,

$$\mathbf{R} = yy^H, \tag{5.25}$$

$$\mathbf{R} = \mathbf{QSQ}^*. \tag{5.26}$$

Where,"*" shows the hermitian transpose of a matrix, $y$ is the down-converted and filtered version of the received signal at the all hydrophones in the array over specific duration of time such as one preamble length, $\mathbf{S}$ shows the eigen values of the matrix $\mathbf{R}$, which is a diagonal matrix that with elements which are decreasing from the first row down to the last row. Based on the desired signal subspace, we can form $\mathbf{Q}_s$ corresponding to the $M$ largest values of $\mathbf{S}$, called signal subspace. Now it is time to define $\mathbf{Q}_0$ and $\mathbf{Q}_1$ derived from $\mathbf{Q}_s$. These two matrices are formed in the same way that $\mathbf{A}_0$ and $\mathbf{A}_1$ are formed.

$$\mathbf{Q}_0 = \mathbf{A}_0\mathbf{C}, \tag{5.27}$$

$$\mathbf{Q}_1 = \mathbf{A}_1\mathbf{C}, \tag{5.28}$$

$$\mathbf{A}_1 = \mathbf{A}_0\Phi. \tag{5.29}$$

$$\mathbf{Q}_0 = \mathbf{Q}_1\Gamma^{-1}, \tag{5.30}$$

$$\Gamma^{-1} = \mathbf{C}^{-1}\Phi^{-1}\mathbf{C}. \tag{5.31}$$

Where, $\mathbf{C}$ is an invertible matrix.

By means of finding the eigenvalues of $\Gamma^{-1}$, and using Eq. 5.24, we are able to find the angles of the arriving signals. The ESPRIT algorithm performance is not good. First, its performance may degrade when we have fewer sensors (hydrophones) than the number of arriving signals. Esprit is also a time consuming method due to the need for calculating two eigenvalue decompositions and a least square problem to find the angles. Hence, we are looking for an algorithm which does not have these two downsides.

### 5.6.2 MUltiple SIgnal Classification (MUSIC)

Since one of the most important algorithm discussed in this thesis is based on the MUSIC algorithm, it is appropriate to show a flow chart for MUSIC algorithm shown in Fig. 5.5. In addition, it is helpful to revise how received signals are formed. The Matlab code regarding the

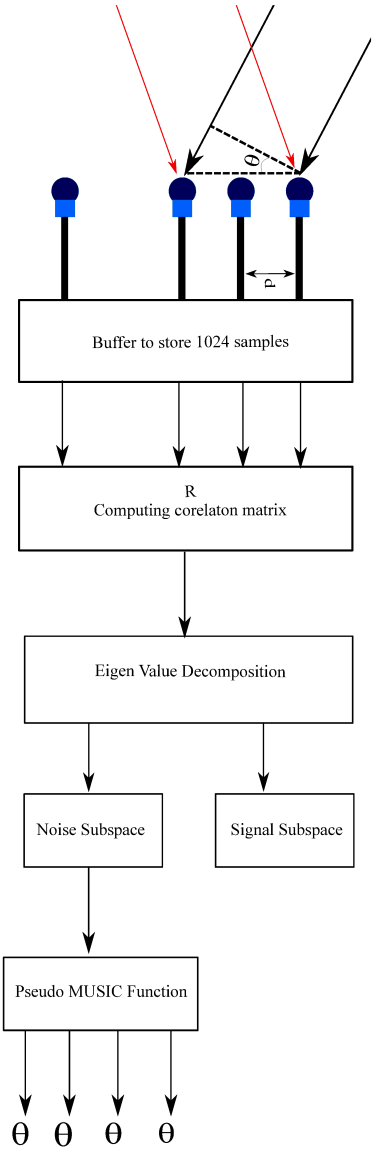


**Figure 5.5:** Hydrophone array

MUSIC algorithm is attached to Appendix B. The received signal at the receiver hydrophone array is affected by the features of the underwater channel. The MUSIC algorithm is based on the orthogonality of steering vector and noise. It searches for the angle of arrivals at which the receiver picks up signal energy. Before explaining the algorithm, it is helpful to describe what the received signal is. This is also explained in Chapter 3.

In this thesis we only consider narrow-band signals with different angles of arrival. The distance between hydrophones $d$ introduces a delay and phase change with regard to the incident

angle of arrival. Eq. 5.32 and Eq. 5.34 describe the received signal, resulting from the transmitted signal $x(t)$ passing through multi-path underwater acoustic channel.

$$y_i(t) = \sum_{p=1}^{L_\mathrm{p}} e^{-j2\pi f_c \frac{d\sin(\theta_p)}{c}} f_p^{(i)}(t) x(t - \Delta t_{i,p} - \tau_p) + n_i(t), \tag{5.32}$$

$$= \sum_{k} \sum_{p=1}^{L_\mathrm{p}} a(\theta_p) f_p^{(i)}(t) g_\mathrm{total}(t - \Delta t_{i,p} - \tau_p - kT) x_k + n_i(t), \tag{5.33}$$

where, $y_i(t)$ is the received signal at hydrophone $i$, $f_p^{(i)}$ models the fading and Doppler spread for path $p$, $L_P$ is the number of paths, and $T$ is the sampling time. $i = 1, 2, \cdots, N_\mathrm{h}$, is the hydrophone index, and the first hydrophone is used as the reference hydrophone when computing the delays associated with hydrophone $i$ which is given as

$$\Delta t_{i,p} = d\sin(\theta_p)(i-1)/c \ . \tag{5.34}$$

The following equation (Eq.5.35) represents the steering vector which is used to steer the beamformer's main-lobe toward the signals arriving from angle $\theta_j$. As it is shown in Eq.5.32 there is a phase shift with regard to hydrophone spacing. This phase shift is going to be canceled by multiplying conjugate of the vector $a(\theta_p)$ which is encapsulated in the received signal $\boldsymbol{y}_i = [y_1(t), y_2(t), ..., y_{N_T}(t)]$. Conjugate of $a(\theta_p)$ is known as steering vector. Thus, by multiplying the steering vector with the received signal, we can cancel the phase shift occurring due to the hydrophone spacing, and align all hydrophones' signals with respect ot their phase.

$$\boldsymbol{a}_{\theta'}(d, \theta_p) = [a_{\theta',1}, a_{\theta',2}, \cdots, a_{\theta',N_\mathrm{h}}]^\mathrm{T} \tag{5.35}$$

$$a_{\theta',i}(d, \theta_p) = e^{j2\pi f_c d\sin(\theta')(i-1)/c} \quad i = 1, 2, \cdots, N_\mathrm{h} \tag{5.36}$$

where, $d$ is the hydrophone spacing, $\theta'$ is the desired signal angle of arrival, $f_c$ is the carrier frequency, and $c$ is the sound speed in the medium.

The MUSIC algorithm[13] [14] relies on the received signal, $\boldsymbol{y}(t)$, correlation matrix $\mathbf{R}$. A

practical way for computing $\mathbf{R}$ is to transmit a known preamble $\boldsymbol{p}$ of length $N_{\text{pre}}$ samples over the channel and to compute $\mathbf{R}$ as an expectation over the $N_{\text{pre}}$ samples of the received vectors corresponding to the preamble only, i.e,

$$\mathbf{R} = \frac{1}{N_{\text{pre}}} \sum_{k=1}^{N_{\text{pre}}} \boldsymbol{y}(kT)\boldsymbol{y}(kT)^* \ . \tag{5.37}$$

Then, an eigen value decomposition is applied to the correlation matrix $\mathbf{R}$ which can be broken up into multiplication of three matrices $\mathbf{R}$=$\mathbf{QSQ}^*$. The matrix $\mathbf{S}$ contains eigen values of the matrix $\mathbf{R}$, and is a diagonal matrix with diagonal elements which decrease from the first row down to the last row. This allows us to identify two subspaces based on diagonal values. Noise subspace in matrix $\mathbf{S}$ is the smaller diagonal elements of the matrix $\mathbf{S}$.

$$\mathbf{S} = \begin{bmatrix} s_1 & 0 & ... & 0 \\ 0 & s_2 & ... & 0 \\ 0 & 0 & ... & 0 \\ . & . & ... & . \\ 0 & 0 & ... & s_{N_h} \end{bmatrix} \tag{5.38}$$

$$\mathbf{S}_s = \begin{bmatrix} s_1 & ... & 0 & ... & 0 & 0 \\ 0 & s_2 & ... & 0 & ... & 0 \\ . & . & ... & . & & \\ 0 & 0 & ... & s_k & ... & ... \end{bmatrix} \tag{5.39}$$

$$\mathbf{S}_n = \begin{bmatrix} 0 & ... & s_{k+1} & ... & 0 & 0 \\ 0 & ... & 0 & s_{k+2} & ... & 0 \\ . & . & ... & . & & \\ 0 & 0 & ... & ... & ... & s_{N_h} \end{bmatrix} \tag{5.40}$$

Then, based on that row separation, we can divide the $\mathbf{Q}$ matrix into two matrices, $\mathbf{Q}_s$ and $\mathbf{Q}_n$, which are signal and noise subspace in $\mathbf{Q}$, respectively.

In the MUSIC algorithm, we have to decide where to cut the $\mathbf{S}$ matrix and make the signal and noise subspaces. Let's assume $\mathbf{S}$ has $N_h$ rows of with $k$ rows belonging to the signal subspace and $N_h - k$ are related to the noise subspace. If we use this separation in $\mathbf{Q}$ the noise

eigenvectors will be called $\mathbf{E}_N$ and are rows $k+1$ to $N_h$ of $\mathbf{Q}$.

The MUSIC algorithm uses different angle, in an interval such as $-60° < \theta < 60°$, for the steering vector $\mathbf{a}(\theta)$ to find the pseudo MUSIC spectrum called PMU($\theta$) as illustrated below

$$\text{PMU}(\theta) = \frac{1}{\mathbf{a}(\theta)^H \mathbf{E}_N \mathbf{E}_N^H \mathbf{a}(\theta)}. \tag{5.41}$$

Since the noise subspace is orthogonal to the steering vectors, a maximum in 5.41 occurs when the denominator reaches a minimum. These minima correspond to the angles at which signal energy arrives. Precision of MUSIC, however, is prone to many factors ranging from SNR to the number of samples to which MUSIC is applied and the ratio between the number of arrival angles and the number of hydrophones. All of these effects are discussed in this section.

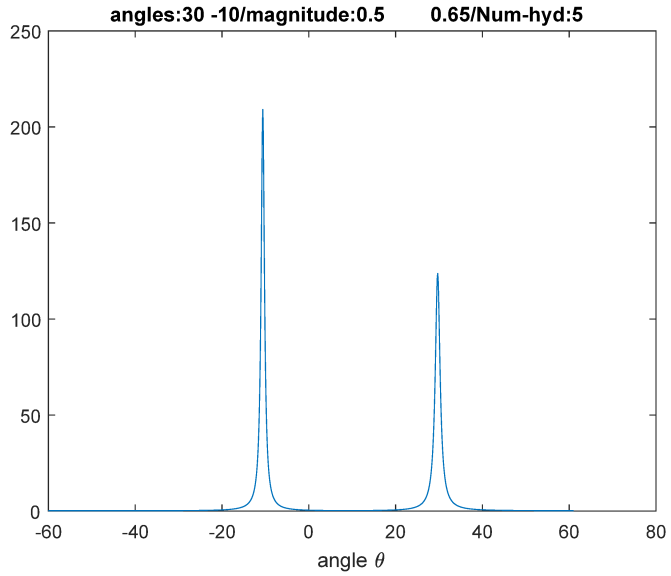


**Figure 5.6:** MUSIC Result for a Matlab test experiment which 5 hydrophones were in the array, the test signals come from angles -10 and 30 degrees, and the SNR = 20 dB.

### 5.6.3 Parameters related to MUSIC Performance

#### Number of Hydrophones

The more hydrophones available in the array, the more accurate the estimation will be. The MUSIC algorithm depends on the number of hydrophones and it can estimate only a number of arrivals which are less than the number of hydrophones. The results for different number of hydrophones is shown in Fig. 5.8.

#### Number of Samples

Since the MUSIC algorithm computes the correlation matrix $\mathbf{R}$, more samples help us have better statistics which leads to more accurate results. As Fig 5.9 shows, even with low SNR and with few number of hydrophones, MUSIC is still able to detect the angles of arrivals.

#### SNR Influence

Higher SNR provides better estimation. In MUSIC algorithm, this is also true. It can be concluded that higher SNR leads to an increase in the precision of the estimation even with fewer samples and numbers of hydrophones placed in the array. Fig 5.10 illustrates how different SNR values cause better estimation.

#### Doppler Spread Effect

As Fig. 5.11 shows, if the Doppler spread increases, the MUSIC precision decreases, even for large numbers of hydrophones. In our simulation, Doppler spread for each path is dependent on number of top bounces, as postulated in [5].

Based on all of these factors, we have to find a way to alleviate their impacts on the MUSIC algorithm result. Therefore,in order to have more samples, we decided to use a probe signal of length 1024 which is 16 copies of a pilot comb $P$ which is a size 64. Thus, the preamble size is 1024. Both preamble and pilot comb are discussed in the Channel Modeling section in Chapter 3. Unfortunately, in the reality we do not know the number of arrivals. Moreover, it is costly to deploy many hydrophones in the array. Although we know that having fewer hydrophones reduces the MUSIC algorithm precision, we found a way to have fewer hydrophones, and still have reliable estimation. This method gives us the opportunity to find the most effective paths,

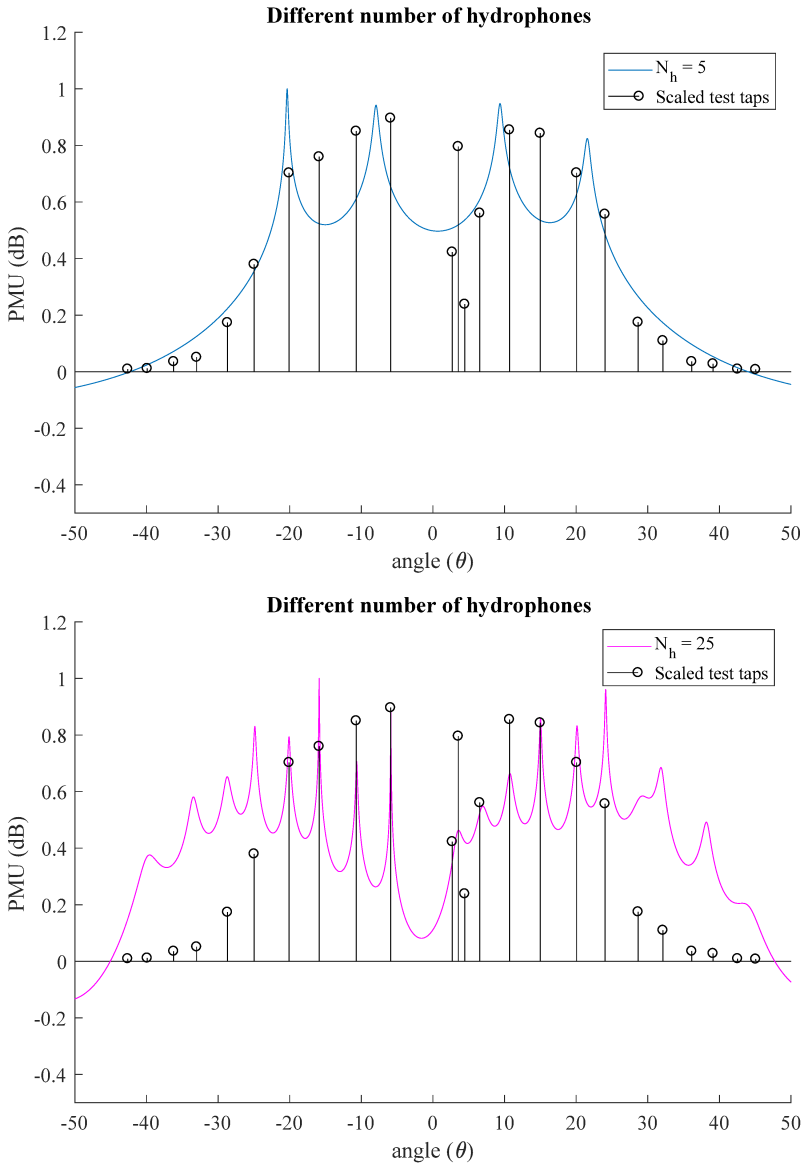


**Figure 5.7:** Results for different numbers of hydrophones, SNR value = 20 dB, no Doppler effect ($\alpha = 0$), and preamble length = 256.

but not all of them. The paths' features which we intent on finding are, first, carrying high energy signals and second, having low Doppler spread.

Separating the signal subspace from the noise subspace is an important procedure. The diagonal values in the matrix **S** shows the distribution of energy in the channel. Since we want to eliminate the low energy paths, we decided to cut the **S** matrix from the rows which shows

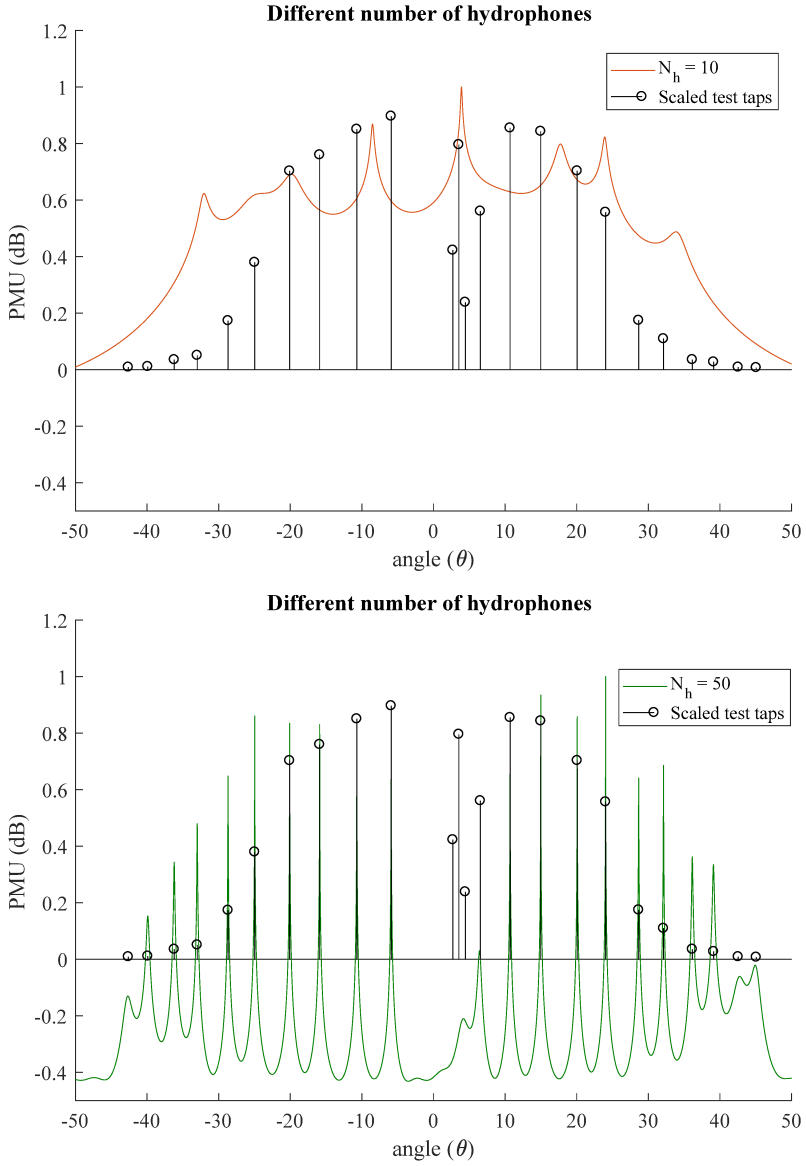


**Figure 5.8:** Results for different numbers of hydrophones, SNR value = 20 dB, no Doppler effect ($\alpha = 0$), and preamble length = 256.

higher values, even if we do not have enough number of hydrophones. Because those paths are the desired paths and rest of the paths can be considered as interference, and can be regarded as noise subspace. Based on this separation, we found that the row at which we separate, plays an important role in the MUSIC algorithm angle estimation. Because when we cut the **S**, which is $5 \times 5$ matrix in our case because our array consists of 5 hydrophones, from the fifth row it detects paths which some of them were moving during different experiments with the same setup. It also

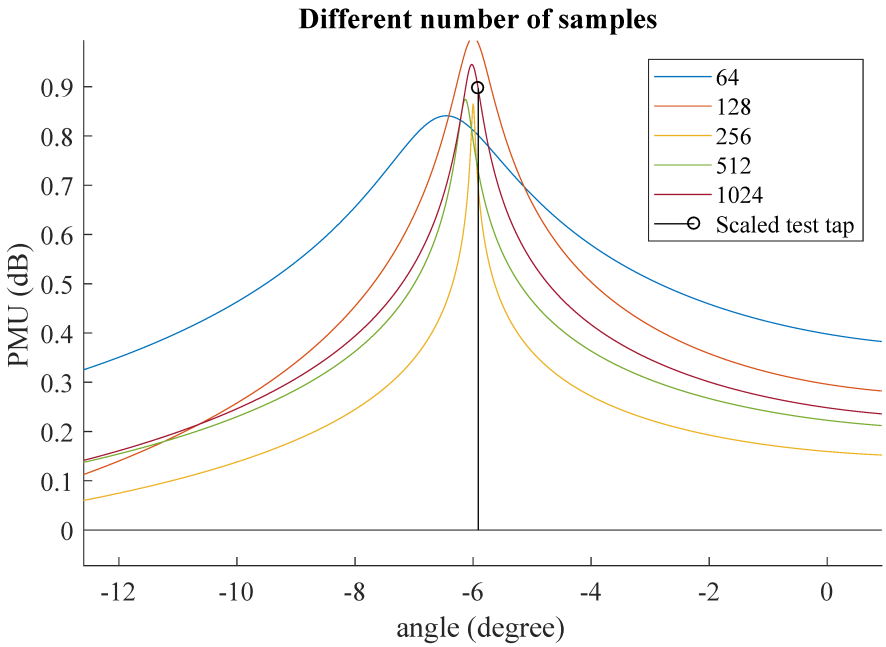


**Figure 5.9:** Larger number of samples improve the MUSIC algorithm accuracy, SNR = 5 dB, no Doppler effect ($\alpha = 0$) and $N_h = 5$.

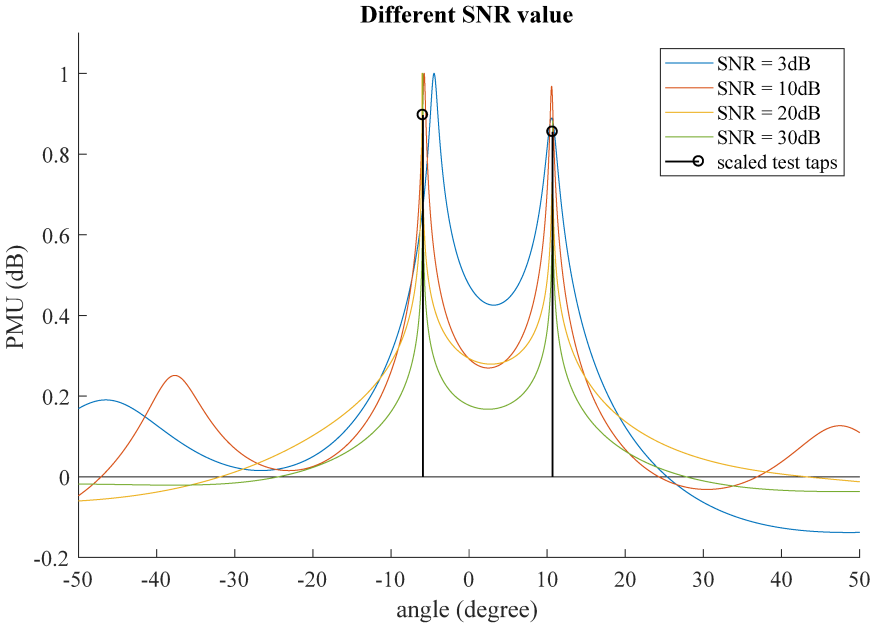


**Figure 5.10:** Higher SNR value results in better estimation, number of samples = 64, $N_h = 5$ and no Doppler effect ($\alpha = 0$).

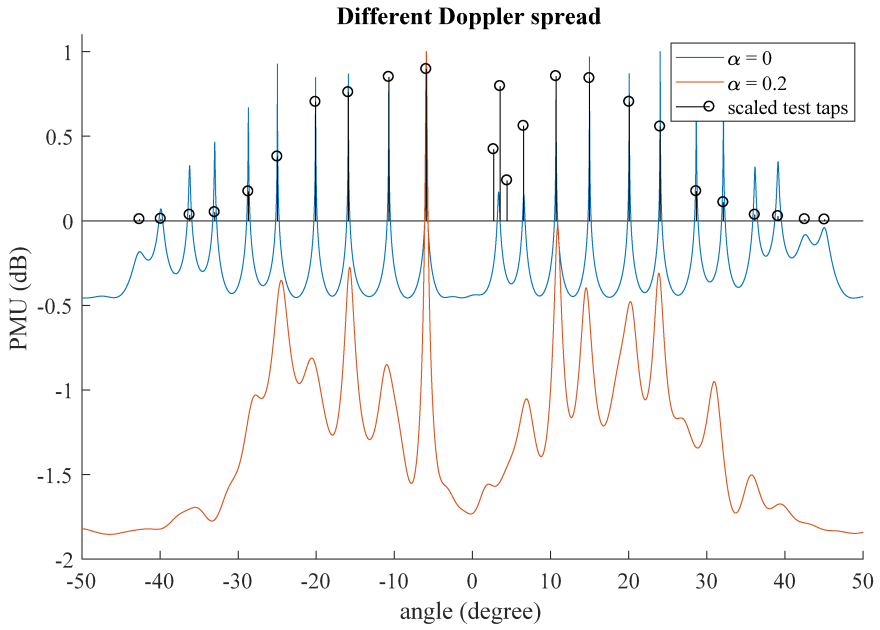


**Figure 5.11:** Different Doppler spread values affect estimation precision, SNR = 20 dB, $N_h = 50$ and number of samples = 256.

detects the paths which do not have good quality based on our criteria. On the other hand, when we cut the **S** matrix from the rows in the **S** which has higher values, say second or third row, we saw that MUSIC shows better estimation accuracy without those moving paths we had faced.

Next, in order to overcome the paths with higher Doppler spread factors, we decided to chop the 1024 received samples into smaller length samples, which in this work we call them sub-symbols, and average all sub-symbols. Exactly the reverse idea which we had for increasing number of samples. In order to lessen the effect of high Doppler paths, we summed those 16 sub-symbols which have length 64. Since high Doppler paths have more non-coherent variations, when we add and average them, those high Doppler paths are added destructively. In fact, those variations cancel the effect of high-Doppler path considerably. On the other hand, paths having low Doppler are be added and averaged constructively. The formulas regarding this technique are shown below. Fig. 5.12 shows diagonal values of **S** before and after averaging.

$$\mathbf{x} = [P_1, P_2, ..., P_{16}], \tag{5.42}$$

$$P_0 = P_1 = ... = P_{16}. \tag{5.43}$$

$$\mathbf{y}_{avg} = \sum_{k=1}^{16} \mathbf{y}_k = \sum_{k=1}^{16} \mathbf{H}_k P_k + n, \tag{5.44}$$

Fig. 5.12 and Fig. 5.13 show the improved estimation based on averaging technique. The diagonal values of **S** matrix are related to signal power. Therefore, in order to focus on those high power and low Doppler path, we cut the **S** at the third row.

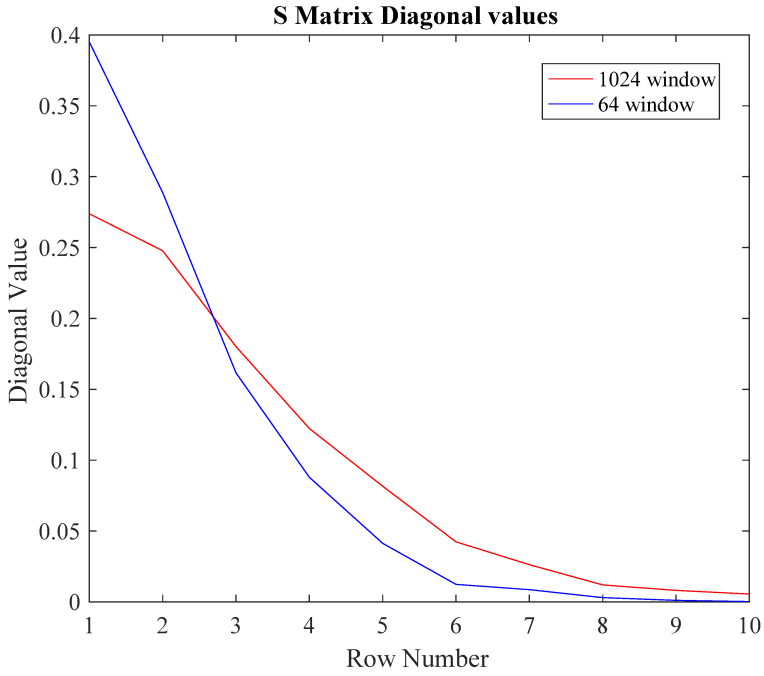


**Figure 5.12:** The decreasing trend in the diagonal values of **S** matrix for 10 hydrophones. Blue line is for averaging, red is before averaging.

There are other types of improved versions of MUSIC algorithm mentioned in the references [21]. They improved MUSIC algorithm results, but based on [21], even those algorithms require more hydrophones than the number of arriving signals. Thus, the proposed averaging technique helps us find the best angles. The effect of averaging for $N_h = 50$ is shown in fig.5.14.

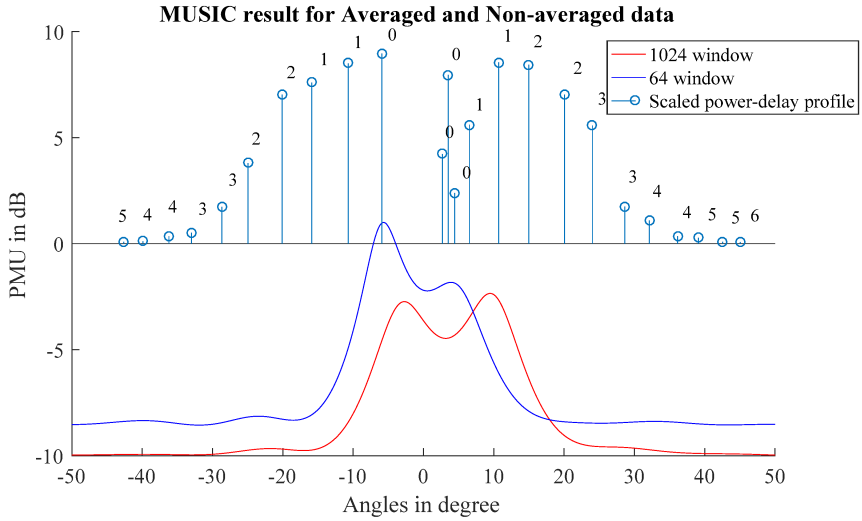


**Figure 5.13:** MUSIC result for averaged and non-averaged- data, number of bounces are showed above each path.

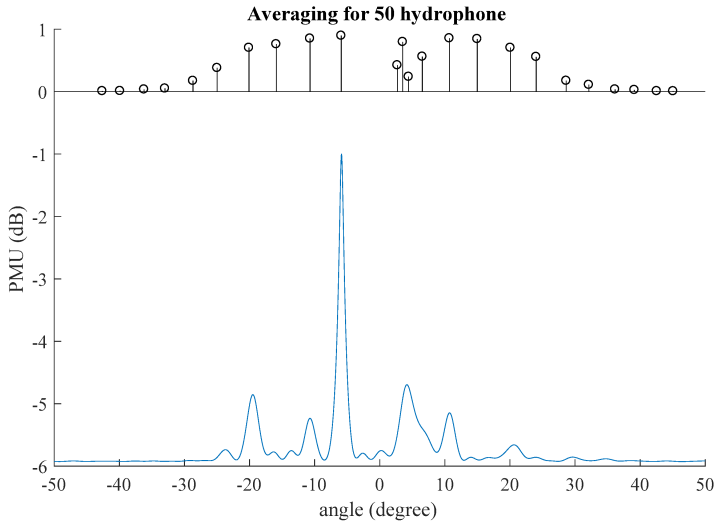


**Figure 5.14:** MUSIC result for averaged received data for 50 hydrophones. Doppler spread $\alpha = 0.1$.

## 5.7 Beamformer Simulation Results

The quality of channel can be quantitatively defined by the RMS delay parameter introduced in Chapter 3. As table 5.1 shows RMS Doppler is considerably small in both cases which 5 and 50 hydrophone were used. Fig. 5.15 shows beamfomred channel based on Bellhop simulation.

| SNR (dB) | 10 | 20 | 30 |
|---|---|---|---|
| MSE (non-beamformed) | 0.1287 | 0.0721 | 0.0683 |
| MSE (beamformed) | 0.0515 | 0.0262 | 0.0226 |
| RMS Delay (non-beamformed) | 0.54607 | | |
| RMS Delay (beamformed) | 0.03412 | | |
| RMS Doppler (non-beamformed) | 1.9136 | | |
| RMS Doppler (beamformed) | 0.1195 | | |

**Table 5.1:** Channel parameter improvement obtained via receive beamforming with $N_{\mathrm{h}} = 5$ hydrophones.

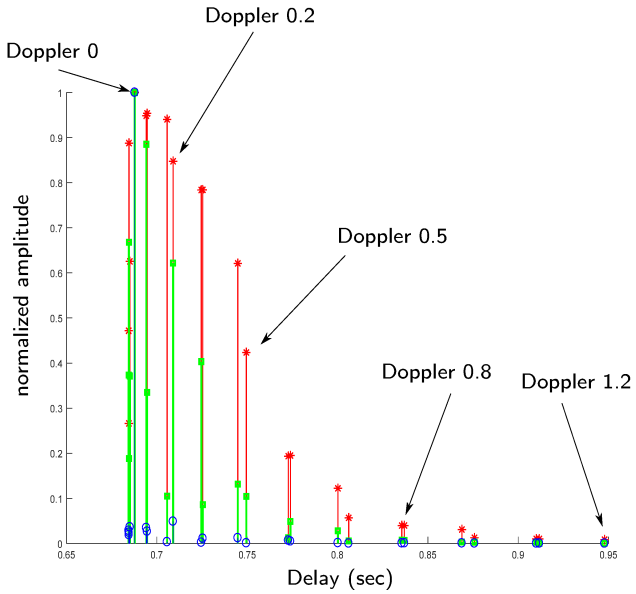


**Figure 5.15:** Beamfomrmed version of the simulated underwater channel (red), the blue taps show the beamforming with 50 hydrophones, and the green taps show the beamformed version of the channel by means of 5 hydrophones.

## 5.8 Beamformer and MUSIC with Measured Data

In this section the application of the delay and sum beamdformer based on MUSIC for real data based on measurements from ocean and Aquatron tests are shown. In the Aquatron the transmitter was placed approximately at 3 meters depth, and the receiver array which had 5 hydrophones, was placed 5 meters away the from the transmitter at the same depth. Fig. 5.18 shows the beamformed versus non-beamformed version of the acoustic channel for calm water. In the ocean test experiment held in July 2017, the transmitter was again placed at 3 meter depth and the receiver array was placed approximately at 3.5 meter. The depth of the water in

that area varies between 6 to 8 meters. The beamformer reduces the RMS-delay parameter as the exact rms-delay is mentioned under each figure for both beamformed and non-beamformed cases.

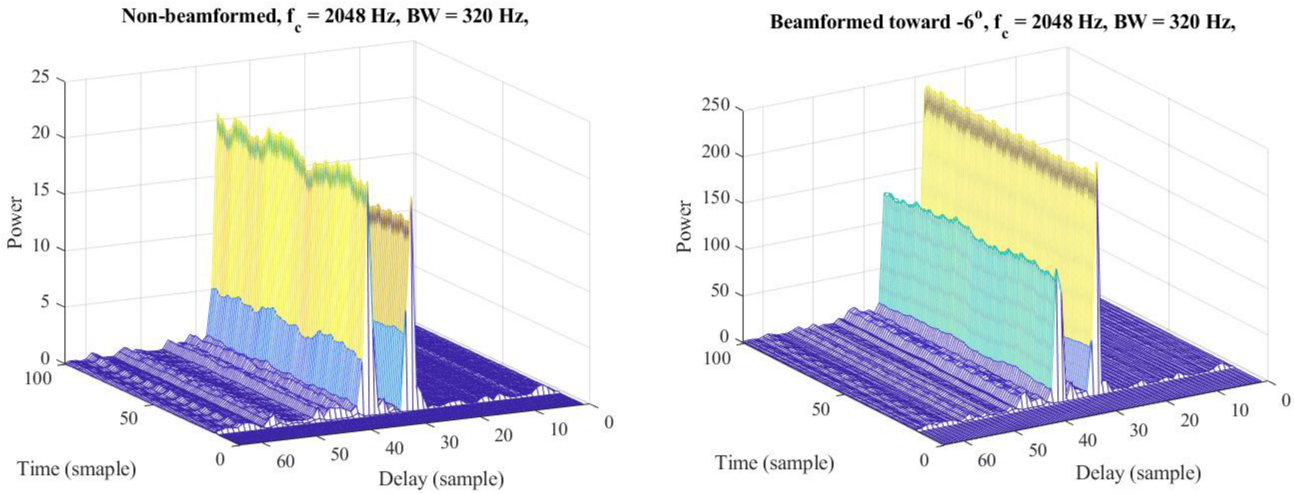


**Figure 5.16:** Real data measurement, the number of hydrophones is 5, distance between hydrophones $d = 36$ cm, carrier frequency $f_c = 2048$ Hz, bandwidth $BW = 320$ Hz, beamformed version of the channel (the left figure) is steered toward -6 degree, the non-beamformed version of the channel (the right figure) is steered toward zero degree. RMS-delay for hydrophone number one is 7.036 sample; however, for beamformed version it is 6.4717 samples.

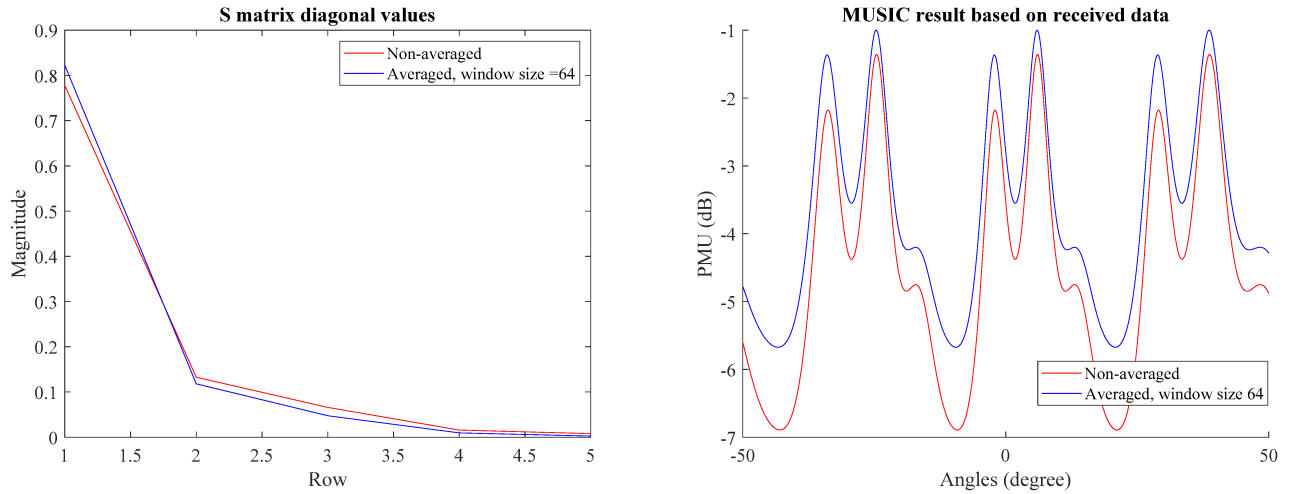


**Figure 5.17:** Real data measurement measured in Atlantic Ocean, the number of hydrophones is 5, distance between hydrophones $d = 36$ cm, carrier frequency $f_c = 8$ kHz, bandwidth $BW = 500$ Hz, the diagonal value of $S$ matrix for averaging method is shown in blue and non-averaged in red (the left figure), the music result based on real data is shown on the right

The ocean experiment which was done in July 2018 in Atlantic ocean close to Peggy's Cove located in Nova Scotia Canada. Weather was windy and ocean was wavy. Since it was windy both boats were drifting with same speed. Therefore, the drift caused Doppler shift, which is compensated in the results shown in the following. The cables which were used in this experiment were not long enough, about 7 meters. Thus, the receiver array was placed in mid-column water which was about 4 meter depth. The depth in that area where the experiment was done was about 7 meters. The transmitter was placed in three different distances, 50,100 and 200 meters away from receiver at 3 meter depth. In the following results for some experiments' results are mentioned.

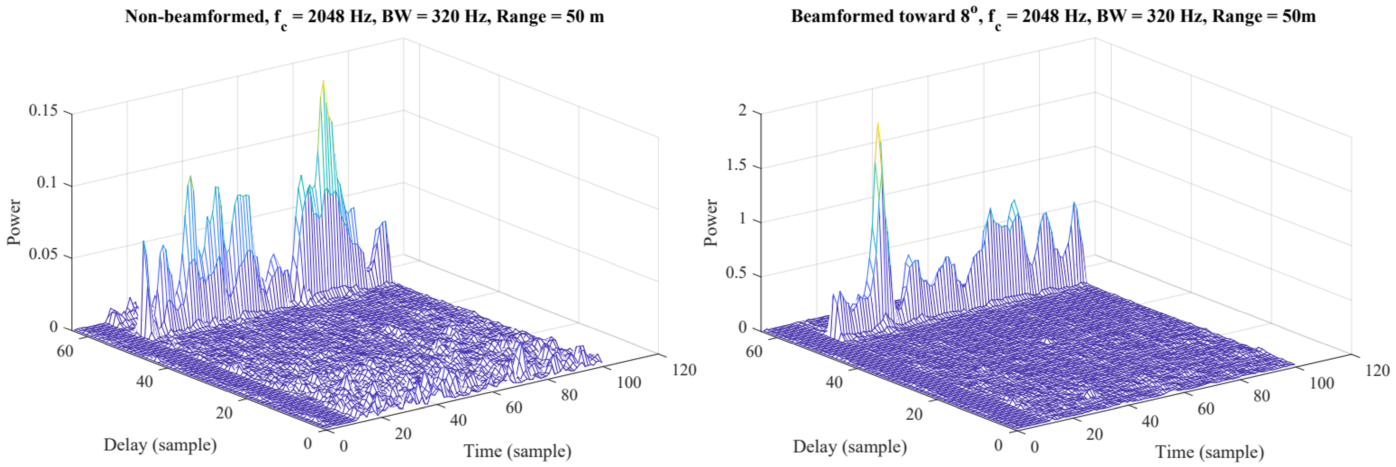


**Figure 5.18:** Real data measurement in the Atlantic Ocean, the number of hydrophones is 5, distance between hydrophones $d = 36$ cm, carrier frequency $f_c = 2048$ Hz, bandwidth $BW = 320$ Hz, beamformed version of the channel (the right figure) is steered toward +8 degree, the non-beamformed version of the channel (the left figure) is steered toward zero degree. RMS-delay for hydrophone number one is 20.3 samples; however, for beamformed version it is 14.7 samples.

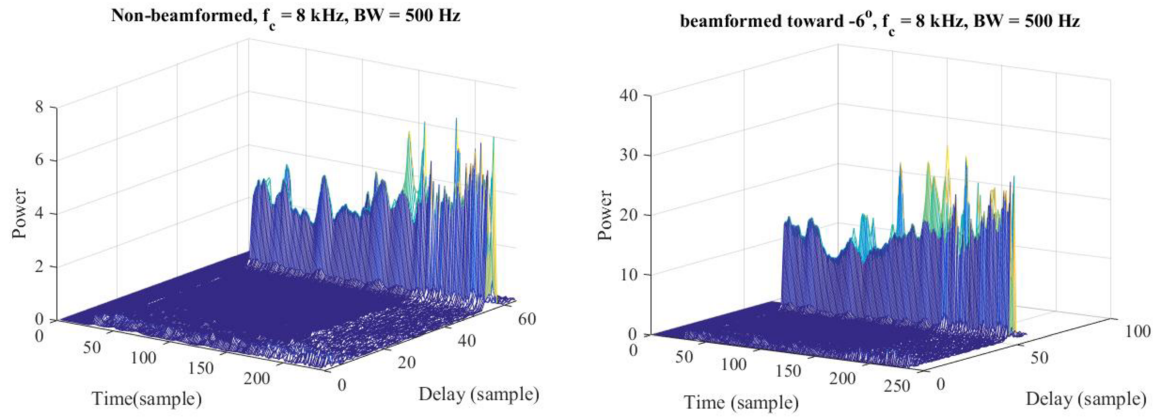


**Figure 5.19:** Real data measurement, the number of hydrophones is 5, distance between hydrophones $d = 36$ cm, carrier frequency $f_c = 8$ kHz, bandwidth $BW = 500$ Hz, beamformed version of the channel (the right figure) is steered toward -0.1 degree, the non-beamformed version of the channel (the left figure) is steered toward zero degree. RMS-delay for hydrophone number one is 16.51 samples; however, for beamformed version it is 14.27 samples.

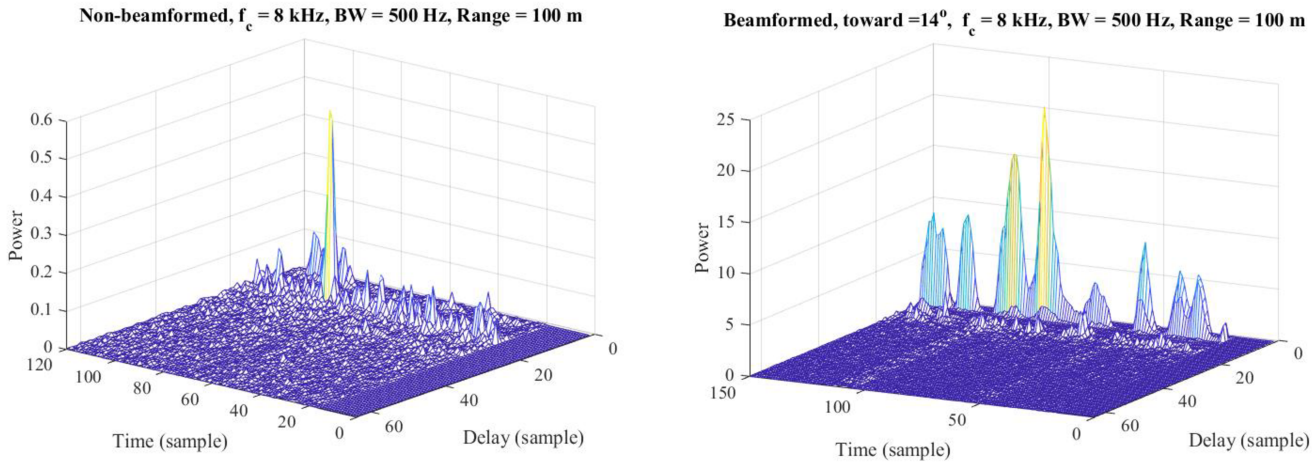


**Figure 5.20:** Real data measurement, the number of hydrophones is 5, distance between hydrophones $d = 36$ cm, carrier frequency $f_c = 8$ kHz, bandwidth $BW = 500$ Hz, beamformed version of the channel (the right figure) is steered toward 14 degree, the non-beamformed version of the channel (the left figure) is steered toward zero degree. RMS-delay for hydrophone number one is 15.74 sample; however, for beamformed version it is 13.25 sample.

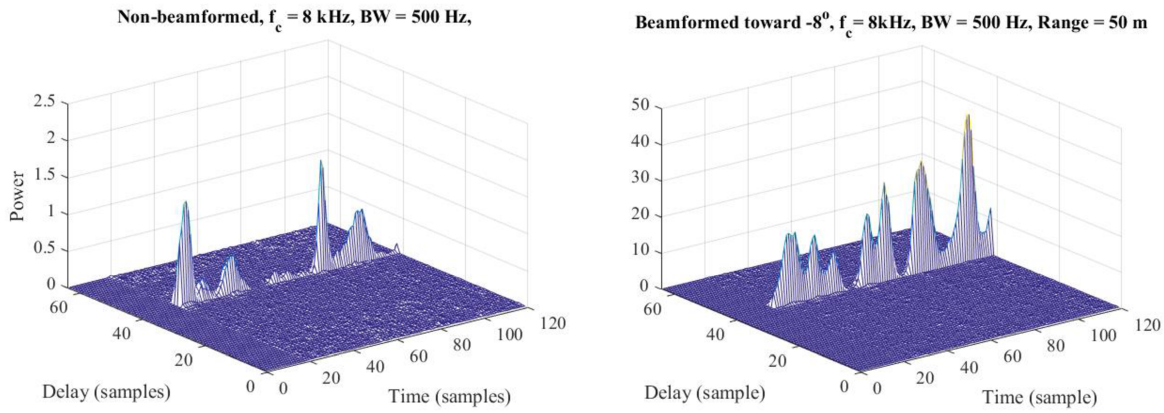


**Figure 5.21:** Real data measurement, the number of hydrophones is 5, distance between hydrophones $d = 36$ cm, carrier frequency $f_c = 8$ kHz, bandwidth $BW = 500$ Hz, beamformed version of the channel (the right figure) is steered toward -8 degree, the non-beamformed version of the channel (the left figure) is steered toward zero degree. RMS-delay for hydrophone number one is 14.24 sample; however, for beamformed version it is 8.89 samples.

# Chapter 6

# Conclusion

## Conclusion

In this thesis we studied how it is possible to improve the channel quality via beamforming techniques. The delay and sum beamformer was applied on both real and simulated data. The underwater acoustic channel performance is measured qualitatively by means of RMS Doppler and RMS delay. DAS beamforming technique shows better results based on RMS delay and RMS Doppler. Both of them are less for the beamformed version of the channel, as shown in chapter 5. DAS beamforming technique requires the knowledge of spatial signature of the signal. Therefore, the multiple signal classification algorithm helps the beamformer adjust its weights to cover the angle of arrival where the desired signal is coming. Concurrently, it suppresses the other arrivals considered as interference.

The performance of the MUSIC algorithm is dependent upon factors such as number of hydrophones in the array, the spacing $d$ between two hydrophone, number of samples, SNR value, and the Doppler spread associated with each path.

Since the number of received paths varies with regard to medium characteristics in which the signal is sent, MUSIC may not be able to estimate all angles of arrival. Therefore, we looked for a method to estimate the best angles of arrival carrying the transmitted signal energy, and having less Doppler spread. Averaging method help MUSIC lessen the effect of high Doppler paths.These paths are added destructively because of significant variation over time samples. Also, the point where the $S$ matrix is divided into noise and signal subspaces should be chosen carefully such that MUSIC only considers low Doppler paths as signal subspace. Fortunately, it increases the MUSIC performance as shown in chapter 5.

**Wide-band Beamforming**

It has been proven that the narrow-band beamfomring techniques are not applicable for wide-band systems. In our case, we use the OFDM signaling which itself is made of several narrow-band signals known as sub-carriers. Therefore, in order to utilize the narrow-band beamforming features, and use larger bandwidth at the same time, it is possible to take Fourier transform and apply the narrow-band beamforming and MUSIC algorithm for each sub-carrier in frequency domain. The received signal in OFDM system can be modeled as,

$$x(t) = \sum_{k=1}^{K} \alpha_k e^{j2\pi f_k t}. \tag{6.1}$$

Since our channel is frequency selective, $\alpha_k$ represents the attenuation for frequency sub-carrier $f_k$. Because of multi-path we receive different replicas of the signal. The received signal at hydrophone number $i$ is

$$y(t) = \sum_{i} \sum_{n=1}^{N_h} x(t - \tau_i - \Delta t_n). \tag{6.2}$$

Where, $\tau_i$ is the delay associated with path $i$, $\Delta t_n$ is the delay associated with hydrophone spacing $d$.

The Fourier transform of the received signal at the hydrophone number $i$ can be shown as,

$$\mathbf{F}\{y(t)\} = \mathbf{Y}(f), \tag{6.3}$$

$$= \sum_{i} \sum_{n=1}^{N_h} \mathbf{F}\{x(t - \tau_i - \Delta t_n)\}, \tag{6.4}$$

$$= \sum_{i} \sum_{n=1}^{N_h} \mathbf{X}(f) e^{j2\pi f \tau_i} e^{j2\pi f \Delta t_n}. \tag{6.5}$$

Where,

$$\mathbf{X}(f) = \sum_{k=1}^{K} \alpha_k \delta(f - f_k). \tag{6.6}$$

Where, $\mathbf{F}$ is the Fourier transform, $\tau$ is the delay associated with each path, and $\Delta t_i$ is the delay caused by hydrophone spacing.

It may be possible to apply the MUSIC algorithm in frequency domain, and find the best angle of arrival for each sub-carrier which is a narrow-band signal. This angle is related to parameter

$\Delta t_i$. By multiplying $e^{-j2\pi f \Delta t_i}$ to Eq. 6.3, The phase shift caused by hydrophone spacing $d$ is canceled. The received signal coming from angle $\theta_i$ will be added constructively, and the rest of arrivals are added destructively over all sub-carriers and all hydrophones in the array.

## Bibliography


[1] N. Eskandari, M. Bashir, D. Truhachev, and C. Schlegel and JF. Bousquet "Improving the Quality of Underwater Acoustic Channel via Beamforming," *IEEE/MTS OCEANS*, Kobe, Japan, May 2018.

[2] B. D. Van Veen and K. M. Buckley, "Beamforming: a versatile approach to spatial filtering," *IEEE ASSP Magazine*, vol. 5, no. 2, pp. 4-24, April 1988.

[3] MUCCI, RA. A comparison of efficient beamforming algorithms. Acoustics, Speech and Signal Processing, IEEE Transactions on. 32. 548 - 558. 10.1109/TASSP.1984.1164359, 1984.

[4] L. Wei and S. Weiss, "Wideband beamforming: concepts and techniques," Wiley, 2010.

[5] P. Qarabaqi and M. Stojanovic, "Statistical characterization and computationally efficient modeling of a class of underwater acoustic communication channels", *IEEE Journal of Oceanic Engineering*, vol. 38, no. 4, pp. 701–717, 2013.

[6] Robert J. Urick. Principles of Underwater Sound 3rd Edition. Peninsula Pub, August 1996.

[7] Siderius, Martin and Porter, Michael and Jensen, Finn. (2001). Impact of thermocline and seabed variability on underwater acoustic communications. Journal of The Acoustical Society of America - J ACOUST SOC AMER. 115. 2469-2469. 10.1121/1.4782437.

[8] M. B. Porter, "Ocean Acoustics Library Bellhop", [online] Available: http://oalib.hlsresearch.com/.

[9] C. Schlegel and M. Jar, "Embedded pilot and multi-size OFDM processing for jointly time and frequency selective channels," *Intern. Symp. on Information Theory and Applications*, pp. 748–752, 2016.

[10] P. A. Van Walree, T. Jenserud, and R. Otnes. "Stretched-exponential Doppler spectra in underwater acoustic communication channels," *The Journal of the Acoustical Society of America*, 2010.

[11] J. C. Peterson and M. B. Porter, "Ray/beam tracing for modeling the effects of ocean and platform dynamics," *IEEE J. Ocean. Eng.,* vol. 38, no. 4, Oct. 2013.

[12] M. Bashir, D. Truhachev, and C. Schlegel, "Kalman Forward-Backward Channel Tracking and Combining for OFDM in Underwater Acoustic Channels," *IEEE/MTS OCEANS*, Kobe, Japan, May 2018.

[13] M. Mohanna, M. L. Rabeh, E. M. Zieur, S. Hekala, "Optimization of MUSIC algorithm for angle of arrival estimation in wireless communications," *NRIAG Journal of Astronomy and Geophysics*, 2013.

[14] T. B. Lavate, V .K. Kokate, and A. M. Sapkal, "Performance analysis of MUSIC and ESPRIT DOA estimation algorithms for adaptive array smart antenna in mobile communication," *International Conference on Computer and Network Technology (ICCNT)*, 2010.

[15] D. Tse and P. Viswanath, "Fundamentals of Wireless Communication" Cambridge University Press, 2005.

[16] P. Hoeher, "A statistical discrete-time model for the WSSUS multipath channel," *IEEE T. Vehicular Tech.*, vol. 41, no. 4, pp. 461–468, 1992.

[17] C. Schlegel et. al., *AIF Quarterly Report*, September 2017.

[18] Au.W.W.L. Hastings, M.C. 2008, XVI, 680 p. 407 illus. ISBN 978-0-387-78364-2 .

[19] R. Coates *Underwater Acoustic Systems*, New York: Springer, 1982. .

[20] http://www.btechacoustics.com/products/bt-25l5 .

[21] http://www.comm.utoronto.ca/∼rsadve
Communication course material notes, Professor Raviraj Adve, university of Toronto.

[22] S. S. Jeng, H. P. Lin, G. Xu and W. J. Vogel, "Measurements of spatial signature of an antenna array," Proceedings of 6th International Symposium on Personal, Indoor and Mobile Radio Communications, Toronto, Ontario, Canada, 1995, pp. 669-672 vol.2. doi: 10.1109/PIMRC.1995.480952

[23] Tie-Jun Shan, M. Wax and T. Kailath, "On spatial smoothing for direction-of-arrival estimation of coherent signals," in IEEE Transactions on Acoustics, Speech, and Signal Processing, vol. 33, no. 4, pp. 806-811, August 1985. doi: 10.1109/TASSP.1985.1164649

[24] S. U. Pillai and B. H. Kwon, "Forward/backward spatial smoothing techniques for coherent signal identification," in IEEE Transactions on Acoustics, Speech, and Signal Processing, vol. 37, no. 1, pp. 8-15, Jan. 1989. doi: 10.1109/29.17496

[25] D. L. Donoho, A. Javanmard and A. Montanari, "Information-Theoretically Optimal Compressed Sensing via Spatial Coupling and Approximate Message Passing," in IEEE Transactions on Information Theory, vol. 59, no. 11, pp. 7434-7464, Nov. 2013. doi: 10.1109/TIT.2013.2274513

[26] D. L. Donoho, "Compressed sensing," in IEEE Transactions on Information Theory, vol. 52, no. 4, pp. 1289-1306, April 2006. doi: 10.1109/TIT.2006.871582

[27] Zhao L, Xu J, Ding J, Liu A, Li L (2017) Direction-of-arrival estimation of multipath signals using independent component analysis and compressive sensing. PLoS ONE 12(7): e0181838. July, 2017

## Appendix A

Increasing Underwater Acoustic channel quality via Beamforming techniques

K301, 1340 Barrington street, Halifax, Nova Scotia, Canada, B3J 1Z1

I am preparing my Masters (MASc) thesis for submission to the Faculty of Graduate Studies at Dalhousie University, Halifax, Nova Scotia, Canada. I am seeking your permission to include a manuscript version of the papers mentioned in Bibliography section as a chapter in the thesis.

Canadian graduate theses are reproduced by the Library and Archives of Canada (formerly National Library of Canada) through a non-exclusive, world-wide license to reproduce, loan, distribute, or sell theses. I am also seeking your permission for the material described above to be reproduced and distributed by the LAC(NLC). Further details about the LAC(NLC) thesis program are available on the LAC(NLC) website (www.nlc-bnc.ca).

Full publication details and a copy of this permission letter will be included in the thesis.

Yours sincerely

Navid Eskandari

Permission is granted for:
a) the inclusion of the material described above in your thesis.
b) for the material described above to be included in the copy of your thesis that is sent to the Library and Archives of Canada (formerly National Library of Canada) for reproduction and distribution.

| | |
|---|---|
| Name: | Title: |
| Signature: | Date: |

# Appendix B

```
% This program aim at finding the best angle of arrival via MUSIC
% algorithm. Then, beamformer based on those angles steers its main-lobe
% toward them. This program is fed with real data.

% Authoer: Navid Eskandari
% Date : 2018-05-03


clear xL;

startpoint = 3000;% the starting sample from which we take 1024 samples

range = startpoint:startpoint+1023;%samples

%x=[x1,x2,x3,x4,x5];

x=[RawWaveBase1([range],1),RawWaveBase2([range],1),RawWaveBase3([range],1),Ra

wWaveBase4([range],1),RawWaveBase5([range],1)];%take the samples from 5

hydrophones

SysPara.fc = 8000;%carrier frequency

R = 0;%initializing the the covariance matrix

c_inv = 1/1500;% inverse of sound speed under the water

SysPara.Rxspacing = 0.36;% the spacing between hydrophones in the array

SysPara.Nr = 5;% number of hydrophones

[Np, SysPara.Nr] = size(x);


for iter = 1:1


    %[trasn,Riter] = corrmtx(x(iter,:),SysPara.Nr-1,'modified');

    R = x'*x;

    %R = Ritter+R;


end

% R = R/PreambleLength;
```

```
[u,s,Q] = svd(R);%singular value decomposition
figure(9)
plot(diag(s)/sum(diag(s)),'r');% plot the diagonal value of the 1024 size
window
%[u1,s1,Q1]=eig(R);
E = Q(:,3:end);% Defining the noise subspace
%E = Q(:,[1]);
[E1,E2] = size(E);% find the size of noise subspace


R1=R;
%%%%%%%%%%%%%%%%%%%%%%%%%%%%%%%%%%%%%%%%%%%%%%%%%%%%%%%%%%%%%%%%%%%%%%%%%%%%
phi = -50:.01:50;
% phi = phi + 90;


for iterphi = 1:length(phi)% different angles
    phivec = - 2*pi * SysPara.fc * c_inv * SysPara.Rxspacing * cos(pi/2 +
phi(iterphi)*pi/180) * (0:SysPara.Nr-1) ;% steering vector
    stear = exp( -1i*phivec );% stearing vector test
%
stear=exp(1i*2*pi*SysPara.fc*c_inv*SysPara.Rxspacing*cos((phi(iterphi))*pi/18
0)*[1:SysPara.Nr]);% stearing vector test
    for iq = 1:E2
        PMU(iq,iterphi)=(stear*E(:,iq)*E(:,iq)'*stear');% denominator of PMU
    end
    PMUs(iterphi)=10*log10(1/abs(sum(PMU(:,iterphi))));%PMU in dB
end


%ang1 = 10.69;
```

```
%phivec = - 2*pi * SysPara.fc * c_inv * SysPara.Rxspacing * cos(ang1*pi/180)
* (0:SysPara.Nr-1)

[pks,locs] = findpeaks(PMUs);% find the peak in PMU
angles = phi(locs)% angle associated with peak
figure(10)
hold on
plot(phi,PMUs,'r')
%%%%%%%%%%%%%%%%%%%%%%%%%%%%%%%%%%%%%%%%%%%%%%%%%%%%%%%%%%%%%%%%%%%%%%%%%%%%
%%%%%%%%%%%%%%%%%%%%%%%%%%%%%% Averaging %%%%%%%%%%%%%%%%%%%%%%%%%%%%%%%%%%%
%Averaging help us remove the high Doppler paths



PreambleLength = 64;% define the size of window
R_2=0;% initializing the R_2 matrix for averaging method
x2 = zeros(PreambleLength,SysPara.Nr);
iter_window = 1;


    for iter_window = 1:(Np/(PreambleLength/16))
        if (PreambleLength *iter_window)<Np
        xL([1:PreambleLength ],[1:5]) = x([(1+PreambleLength *(iter_window-
1)):(PreambleLength *iter_window)],:) ;% averaging based on number of samples
        x2=x2+xL;
        end
    end


x2=x2/(Np/(PreambleLength/16));% averaging
%%%%%%%%%%%%%%%%%%%%%%%%%%%%%%  Correlation matrix  %%%%%%%%%%%%%%%%%%%%%%%%%
```

```
 Riter = x2'*x2;
% [trasn,Riter]=corrmtx(x(:,iter),length(x(:,iter))-1,'modified');
R_2=R_2+Riter;
[u_b,s_b,Q_b]=svd(R_2);% singular value decomposition
%[u1,s1,Q1]=eig(R);
figure(9)
hold on
plot(diag(s_b)/sum(diag(s_b)),'b');
hold off
E_b = Q_b(:,3:end);
%E = Q(:,[1]);
[E1,E2] = size(E_b);
%R1=R;
%%%%%%%%%%%%%%%%%%%%%%%%%%%%%%%%%%%%%%%%%%%%%%%%%%%%%%%%%%%%%%%%%%%%%%%%%%%%%%%
phi_2=(-50:.1:50);
for iterphi = 1:length(phi_2)
    phivec = - 2*pi * SysPara.fc * c_inv * SysPara.Rxspacing * cos(pi/2 +
phi_2(iterphi)*pi/180) * (0:SysPara.Nr-1) ;
    stear = exp( -1i*phivec );% stearing vector test
%
stear=exp(1i*2*pi*f*c_inv*SysPara.Rxspacing*cos((phi(iterphi))*pi/180)*[1:N_h
yd]);% stearing vector test
    for iq = 1:E2
        PMU_2(iq,iterphi)=(stear*E_b(:,iq)*E_b(:,iq)'*stear');%
    end
    PMUs_2(iterphi)=10*log10(1/abs(sum(PMU_2(:,iterphi))));
end
[pks_2,locs_2] = findpeaks(PMUs_2);
angles_2 = phi_2(locs_2)
```

```
figure(10)
hold on
plot(phi_2,PMUs_2/max(PMUs_2),'b')
% polar(phi_2,PMUs_2/max(PMUs_2),'b')
angletest = -6.5;% defining weights for beamformer.
a1 = exp(j*2*pi*SysPara.fc*0.36*1*sin(angletest*pi/180)*(1/1500))
a2 = exp(j*2*pi*SysPara.fc*0.36*2*sin(angletest*pi/180)*(1/1500))
a3 = exp(j*2*pi*SysPara.fc*0.36*3*sin(angletest*pi/180)*(1/1500))
a4 = exp(j*2*pi*SysPara.fc*0.36*4*sin(angletest*pi/180)*(1/1500))
```